AD-A138 839 ULTRASONIC METHODS TO STUDY SHADOW BOUNDARIES OF DIFFRACTING CRACKS ULTRA..(U) OHIO STATE UNIV RESEARCH FOUNDATION COLUMBUS L ADLER FEB 84 MDA903-81-C-0290 1/1

UNCLASSIFIED F/G 14/2 NL

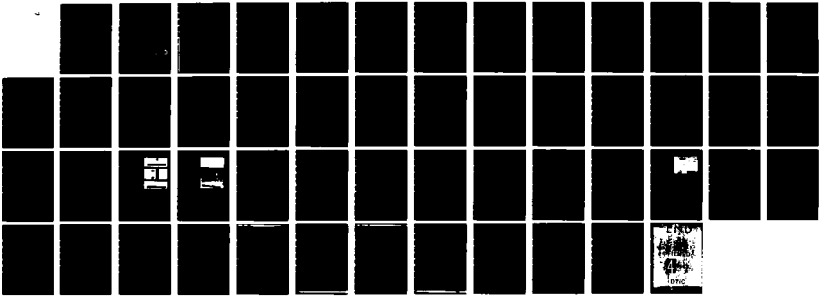

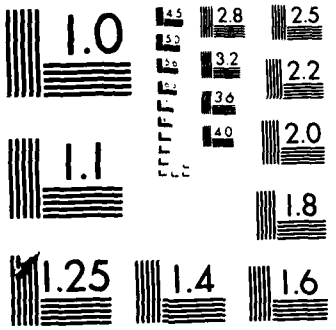

MICROCOPY RESOLUTION TEST CHART
NATIONAL BUREAU OF STANDARDS-1963-A

RF Project 762638/713713
Final Report

ULTRASONIC METHODS TO STUDY SHADOW BOUNDARIES OF DIFFRACTING CRACKS. ULTRASONIC CAUSTICS IN NDE.

Laszlo Adler
Department of Welding Engineering

For the Period
April 1, 1981 - March 31, 1983

DEFENSE ADVANCED RESEARCH PROJECTS AGENCY
1400 Wilson Blvd.
Arlington, VA 22209

Contract No. MDA903-81-C-0290

February, 1984

OSU
The Ohio State University Research Foundation
1314 Kinnear Road
Columbus, Ohio 43212

The views, opinions, and findings contained in this report are those of the author and should not be construed as an official Department of Defense position, policy, or decision, unless so designated by other official documentation.

SECURITY CLASSIFICATION OF THIS PAGE *(When Data Entered)*

REPORT DOCUMENTATION PAGE		READ INSTRUCTIONS BEFORE COMPLETING FORM
1. REPORT NUMBER	2. GOVT ACCESSION NO.	3. RECIPIENT'S CATALOG NUMBER
4. TITLE *(and Subtitle)* ULTRASONIC METHODS TO STUDY SHADOW BOUNDARIES OF DIFFRACTING CRACKS. ULTRASONIC CAUSTICS IN NDE.		5. TYPE OF REPORT & PERIOD COVERED Final Report 4/1/81-3/31/83
		6. PERFORMING ORG. REPORT NUMBER 762638/713713
7. AUTHOR(s) Laszlo Adler		8. CONTRACT OR GRANT NUMBER(s) MDA903-81-C-0290
9. PERFORMING ORGANIZATION NAME AND ADDRESS The Ohio State University Research Foundation, 1314 Kinnear Road Columbus, Ohio 43212		10. PROGRAM ELEMENT, PROJECT, TASK AREA & WORK UNIT NUMBERS 1001/1036
11. CONTROLLING OFFICE NAME AND ADDRESS Defense Advanced Research Projects Agency 1400 Wilson Blvd. Arlington, VA 22209		12. REPORT DATE February, 1984
		13. NUMBER OF PAGES 48
14. MONITORING AGENCY NAME & ADDRESS*(if different from Controlling Office)*		15. SECURITY CLASS. *(of this report)* Unclassified
		15a. DECLASSIFICATION/DOWNGRADING SCHEDULE

16. DISTRIBUTION STATEMENT *(of this Report)*

Approved for public release; distribution unlimited.

17. DISTRIBUTION STATEMENT *(of the abstract entered in Block 20, if different from Report)*

18. SUPPLEMENTARY NOTES

19. KEY WORDS *(Continue on reverse side if necessary and identify by block number)*

non-destructive evaluation, ultrasonic, inversion, defect characterization, shadow boundaries, caustics, defraction

20. ABSTRACT *(Continue on reverse side if necessary and identify by block number)*

The formation of caustics due to the defraction of ultrasound is predicted theoretically and observed experimentally in the shadow region of elliptical discontinuities in material. Good agreement is obtained between experiment and theory. It is suggested to use this method to determine size and orientation of cracks in structural materials, which is an important problem in non-destructive evaluation.

DD FORM 1 JAN 73 1473 EDITION OF 1 NOV 65 IS OBSOLETE

SECURITY CLASSIFICATION OF THIS PAGE *(When Data Entered)*

FINAL REPORT

MDA903-82-C-0290

Submitted to

DEFENSE ADVANCED RESEARCH PROJECTS AGENCY
1400 Wilson Blvd.
Arlington, VA 22209

by

ULTRASONIC NONDESTRUCTIVE EVALUATION GROUP
DEPARTMENTS OF WELDING ENGINEERING & ENGINEERING MECHANICS
THE OHIO STATE UNIVERSITY
190 W. 19th Avenue
Columbus, Ohio 43210

entitled

ULTRASONIC METHODS TO STUDY SHADOW BOUNDARIES OF DIFFRACTING CRACKS. ULTRASONIC CAUSTICS IN NDE.

Submitted by:

Dr. Laszlo Adler, Principal Investigator
Professor of Welding Engineering & Engineering Mechanics
(614) 422-1974

FINAL REPORT

TITLE: Ultrasonic Methods to Study Shadow Boundaries of Diffracting Cracks. Ultrasonic Caustics in N.D.E.

OBJECTIVES OF THE CONTRACT:

The objectives of our research were to investigate ultrasonic methods to reconstruct the field pattern in the shadow region of diffracting cracks in materials to aid quantitative flaw characterization. To develop a theoretical analysis for the inversion of the measured scattered field to obtain size, shape and orientation of material defects. One major factor in this investigation is the interdisciplinary and international scientific and technical interaction. Dr. Peter Doyle, research scientist from the Aeronautical Research Laboratory of Melbourne, Australia is closely interacting with the ultrasonic N.D.E. Group at the Ohio State University. In the following section a summary of theoretical and experimental developments on this project and a list of publications resulted from this project are given.

1. Summary

A new inversion procedure has been developed which relates the geometrical characteristics such as size, shape and orientation of crack-like defects to the envelopes of ultrasonic diffraction caustics which appear in the shadow region of the flaw. An experimental system has been developed which involves a two-dimensional scanning of the ultrasonic field diffracted by the boundaries of discontinuities with a miniature ultrasonic probe. With this system shadow boundaries of circular and elliptical metal discontinuities in water (simulating cracks) has been studied. It is significant to point out that ultrasonic

diffraction caustics have been observed for the first time (see reference). In addition, experimental finding agrees very well with theoretical prediction. It appears that this inversion procedure is sound. It has the potential to develop as a practical nondestructive evaluation method, provided the information about caustics can be carried out from the bulk of a solid material. We carried out one experiment where the flaw was a penny-shaped (circular) crack in a diffusion bonded specimen. and the caustic pattern (which is a point) has been observed. This analysis gave the correct crack dimensions. We have also prepared diffusion bonded samples with non-symmetrical cracks with these planes parallel with the specimen surface as well as cracks with various orientation to the surface. The diffraction caustic patterns of these asymmetrical cracks with nonideal orientation.were also studied.

2. Theoretical Developments

Derived analytical expressions for the diffraction of elastic waves from two-dimensional defects. The expression is valid in the shadow region of the diffracting edge. By using a geometrical theory of diffraction and asymptotic expansion of the diffraction integral, simple equations were obtained to correlate the caustic patterns of defect and its involute which is the diffracting edge itself. For elliptical cracks this formation predicts a caustic pattern which is an astroid. The relative locations of the cusps are related to size, shape and orientation of the crack. The center problem is to find the ultrasonic caustic pattern of the diffracting edge of the crack. No such findings have been reported previously in the open literature.

3. Experimental Developments

The most challenging problem for the experimental development is to find the ultrasonic caustics. These caustics are in the shadow region of the defect and have very small amplitudes. Two types of defects are considered: a) flat elliptical metal composite disks (with air gap between two thin steel plates immersed in water); b) circular cavities in diffusion bonded titanium disks. Although several techniques have been tried out (Bragg Imaging, Schlieren System, Liquid Crystal) the final version of the experimental set-up is shown on Figure 1.

A focussed transducer is excited by a single frequency pulse to provide a point source at the focal point. Care was taken to provide a uniform acoustic field at the point where the diffracting edge is placed. The shadow region is scanned by a specially designed broadband miniature probe with a sensing element of 250 μ in Figure 2. The amplified signal is displayed on a memory scope. A sequency of results are shown on Figure 3 which were taken along the minor axis at various vertical positions. The apparent little "beeps" are the crossing of the caustic envelopes. These are the first observations of the caustics. Agreement between experiment and theory, shown on Figure 4 is very encouraging.

PUBLICATIONS AND PRESENTATIONS

1. "Caustics and the Inversion of Ultrasonic Scattering Data," P. A. Doyle, J. Latimer and L. Adler, Research Techniques in Nondestructive Testing, Vol. V Academic Press, London (1982), Edited by R. S. Sharpe.

2. "Study of Shadow Region of Obstacles by Ultrasonic Diffraction for NDE," Jerry Latimer, P. A. Doyle and Laszlo Adler, J. Acoust. Soc. Am., Vol. 69, 1981.

3. "Ultrasonic Caustics and the Inverse Scattering Problem," P. A. Doyle, J. Latimer and L. Adler, 2nd AIP Applied Physics Conference, Melbourne, November-December, 1981.

4. "Inversion of Scattering Data of the Shadow Region of Discontinuities," Laszlo Adler, Jerry Latimer, Lynn Congos and Peter Doyle, Proceedings of the ARPA/ARML Review of Progress in Quantitative NDE, 1981.

5. "Observation of Diffraction Caustics for Ultrasound," Rui-qi Dong and Laszlo Adler, J. Appl. Phys. 54 (5), May 1983, 2832-2834.

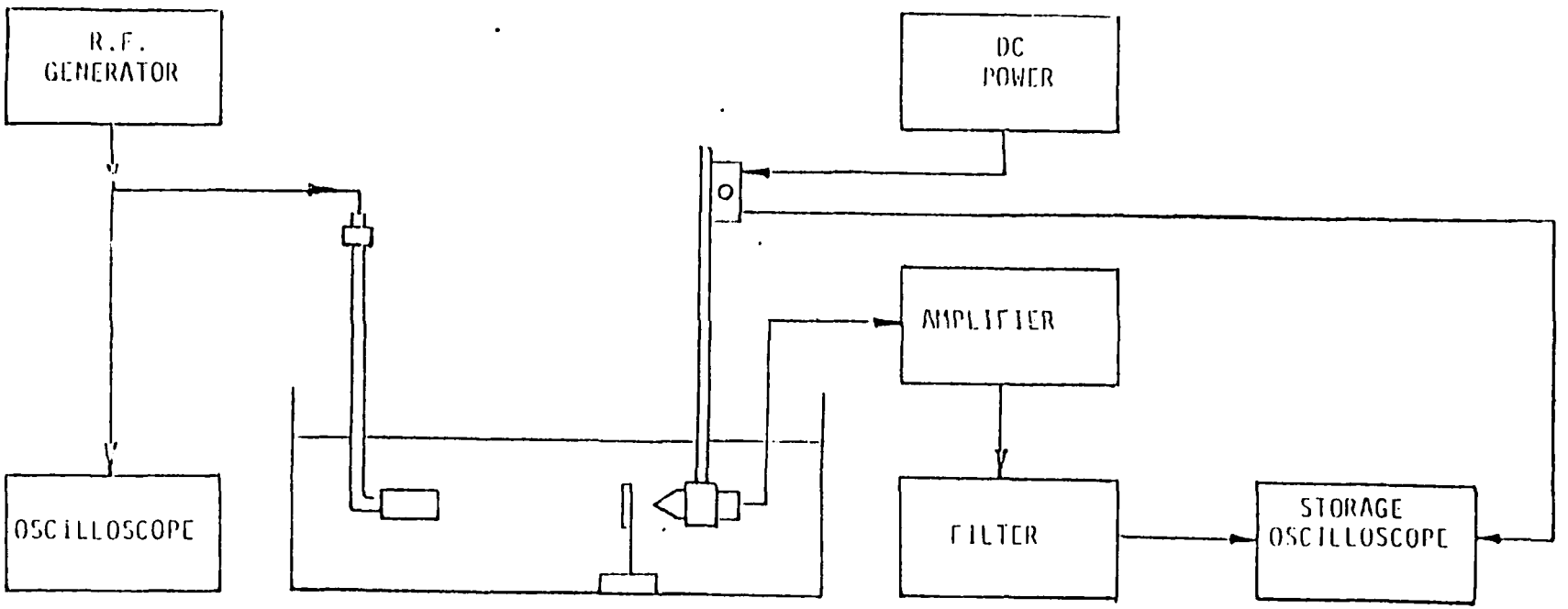

Figure 1. Experimental Arrangement.

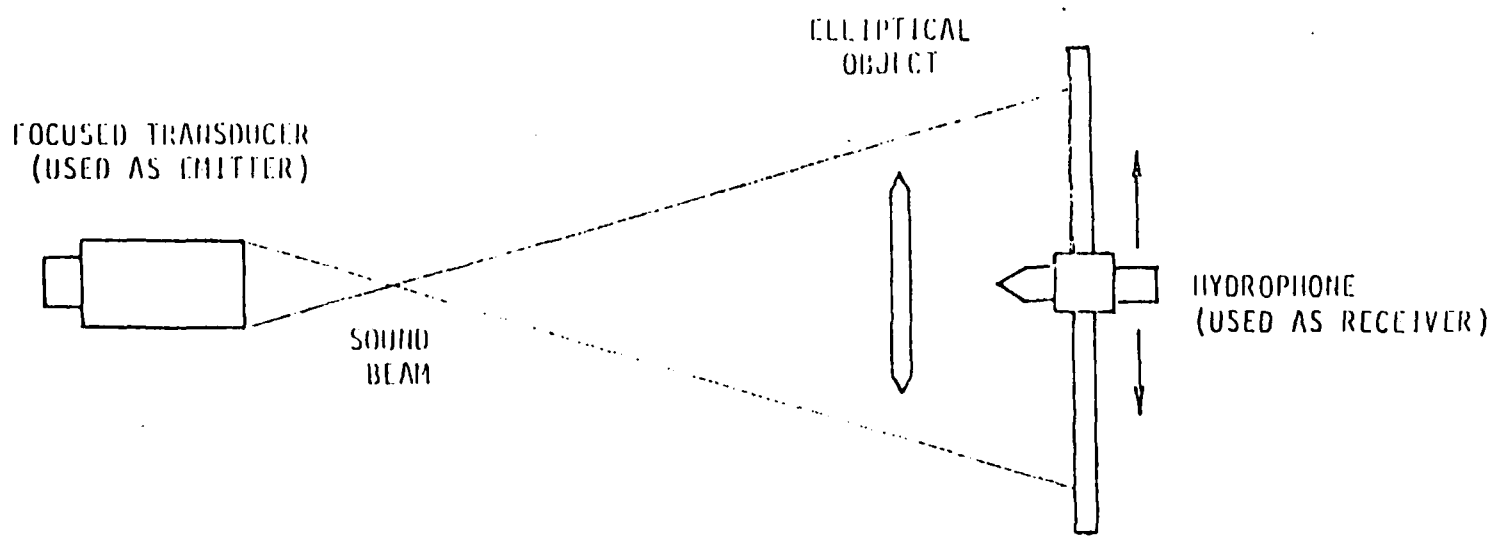

Figure 2. Schematics of the Transducers and Discontinuity.

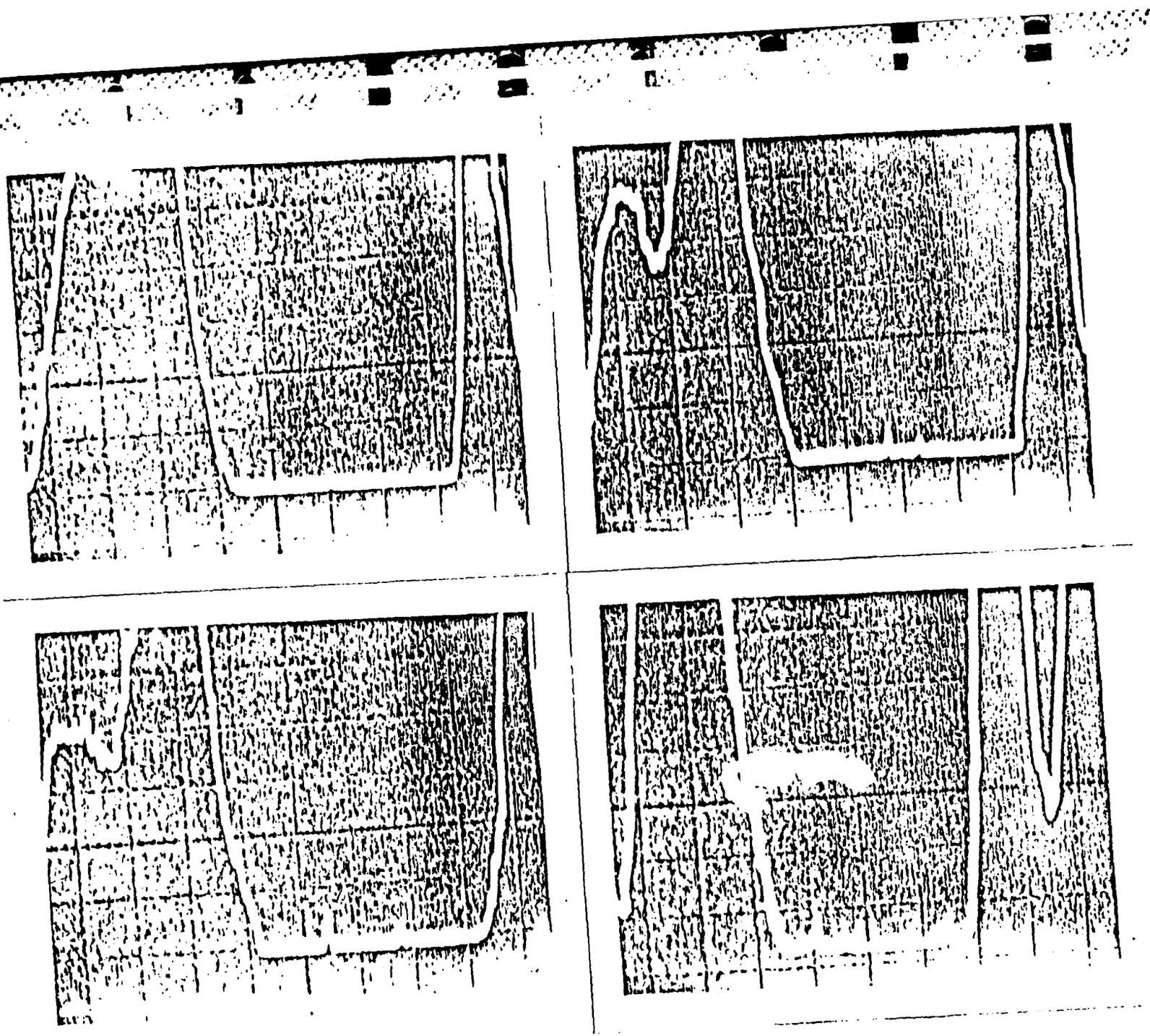

Figure 3. Four Different Positions of Hydrophone Scanning, the Small Signals are obtained in the Shadow Region.

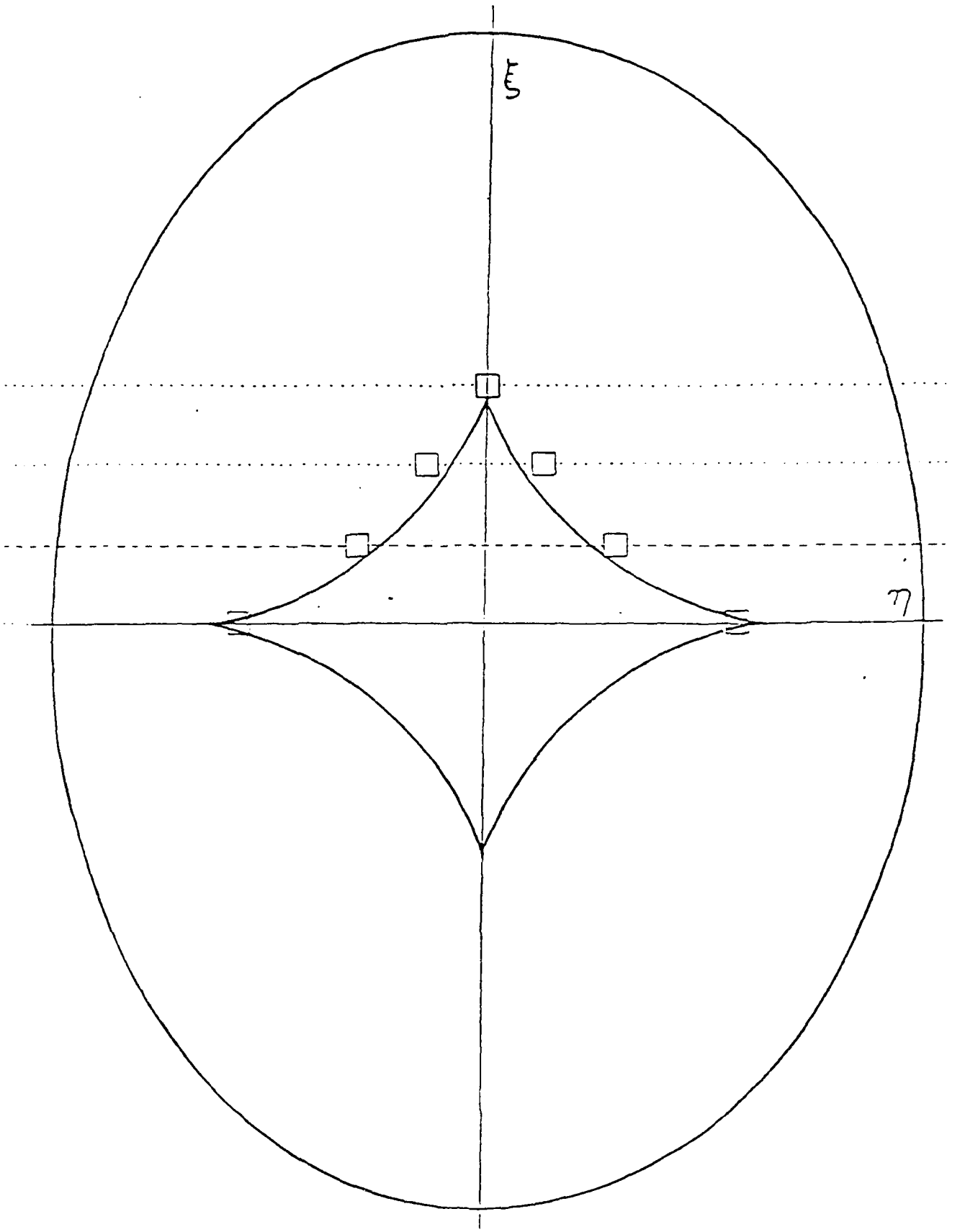

Figure 4. Theoretical (Solid Line) and Experimental Points of Caustics for an Elliptical Crack.

CHAPTER 4

Caustics and the Inversion of Ultrasonic Scattering Data

P. A. DOYLE

Aeronautical Research Laboratories, Department of Defence, Melbourne, Australia

J. LATIMER

Department of Physics and Astronomy, The University of Tennessee, Knoxville, Tennessee, USA

L. ADLER

Departments of Welding Engineering and Engineering Mechanics, Ohio State University, Columbus, Ohio, USA

I. Introduction

It is widely appreciated that as mechanical structures become more complex and expensive, more reliable estimates are required of the initial and residual life of their components, with a known balance between safety and cost contained in those estimates. The role of quantitative ultrasonics is to provide as input for such a lifing scheme the nature, shape, size and orientation of any defects in the components. Ultrasonic and acousto-optical imaging methods, pulse transit-time measurements, scattering experiments including the basic pulse-echo technique, and ultrasonic spectroscopy are the principal approaches adopted to achieve this end.

Recently, attention has been given to the central problem for ultrasonic elastic wave scattering, which is the inversion of scattering data. This article will discuss the possibility of using caustics, which form the envelope of rays diffracted by the defect, to achieve this inversion, as proposed by Doyle (1980). Caustics are well known in optics and have been observed in other fields of scattering, such as molecular collisions (Conner, 1976) and diffuse scattering of X-rays and neutrons by dislocation loops (Trinkaus, 1971). Our primary interest here is in crack-like defects, which need not be planar.

Since no exact solution exists for the inverse scattering problem for elastic waves (nor for the forward scattering problem except in a very few cases), it is appropriate to specify inversion procedures by their particular approximations, and hence their theoretical range of validity. These approximations are often expressed in terms of kl, where k is the wave number and l is a typical dimension of the defect. We here use instead the ratio $l/\lambda = kl/2\pi$ where λ is the wavelength, since the physical implication is then immediately pictured. Our present proposal using caustics applies strictly in the high frequency limit $l/\lambda \gg 1$, and will become progressively less appropriate as l/λ decreases. Other inversion procedures in this regime of l/λ have been proposed by Achenbach *et al.* (1979a, b) using the geometrical theory of diffraction (GTD) for elastic waves (Achenbach and Gautesen, 1976), and by Whalen and Mucciardi (1979) using an adaptive learning approach. These procedures will be discussed and compared with our present proposal using caustics at the end of this article, with particular regard to the likely relative difficulty of extending the techniques from artificial to real cracks.

In Section II, the relevant properties of the caustic surfaces—notably of their goemetry—are extracted formally from the framework of high frequency diffraction theory, which entails the GTD and catastrophe theory. This is done to provide a firm basis for the method, though it should not obscure the essential simplicity of the geometrical inversion procedure using caustics, which is described in Section III. In Section IV, after first showing theoretically that ultrasonic caustics should be observable with careful technique, we

present our preliminary experimental observations using artificial scatterers. The discussion of Section V gives general properties of caustics from voids and inclusions, and then makes the comparison with other inversion procedures mentioned above.

II. Theory for Crack-like Defects

The case of most practical importance in NDT concerns the scattering of elastic waves by defects in solids. However, it will be shown below that the geometry of the caustic surfaces for elastic waves can readily be inferred from that of caustics in the scalar wave case. Since the inversion procedure described here relies solely on a knowledge of the caustic geometry, requiring no quantitative data on the amplitude and phase of the diffracted waves, we need only consider solutions for the scattered wave amplitude u of the reduced scalar wave equation

$$\Delta u + k^2 u = 0 \tag{1}$$

Diffraction by the edge of a two-dimensional crack-like defect, which in general is not planar, will be considered in this section. The host material away from the defect is taken to be homogeneous and isotropic. The radius of curvature at all points on the edge is assumed to be large compared with the wavelength; therefore we are concerned with solutions of eqn (1) asymptotic with respect to k. It will be useful to consider firstly the origins of the geometrical theory of diffraction.

A. The Geometrical Theory of Diffraction of Keller

When an exact solution of eqn (1) exists, its high frequency behaviour can be studied by expanding asymptotically in k. When no exact solution exists, the Luneburg-Kline series (Kline and Kay, 1965) provides a direct method, using the rays of geometrical optics, to construct an asymptotic solution at the field point y in the form

$$u(\mathbf{y}) \sim \exp[ik\phi(\mathbf{y})] \sum_{m=0}^{\infty} (ik)^{-m} z_m(\mathbf{y}), \quad k \to \infty \tag{2}$$

Inserting eqn (2) into eqn (1) gives the eikonal equation for the phase function $\phi(\mathbf{y})$ and a recursive set of transport equations for the amplitude functions $z_m(\mathbf{y})$. However, while the Luneburg–Kline series can describe reflection and refraction, it cannot without modification describe diffraction. One way to see this is to note that available exact solutions for diffraction problems (e.g. the half-plane result of Sommerfield, 1954) characteristically involve half-integral powers of k, which are absent from eqn (2).

point $\mathbf{x}(s)$. The first and most important term of the modified series for u is

$$u \sim D[\gamma/(\gamma+\sigma)\sigma]^{\frac{1}{2}} \exp[ik\phi(\sigma, s)] \tag{4}$$

where γ is the distance from the point $\mathbf{x}$ to the other caustic along the ray (the edge itself is one caustic of the astigmatic pencil of diffracted rays, which is another reason why the Luneburg–Kline series does not describe diffraction). The diffraction coefficient D is found by matching eqn (4) with the solution to the appropriate canonical problem, that is, the simplest problem with the same local goemetry. For diffraction by a smooth edge, the appropriate comparison is with the asymptotic approximation to the exact half-plane result of Sommerfeld (1954). This comparison technique introduces a factor $k^{-\frac{1}{2}}$ which is absent from the unmodified Luneburg–Kline series; it is central to much of the success enjoyed by the GTD.

The factor $[\gamma/(\gamma+\sigma)\sigma]^{\frac{1}{2}}$ is found from the conservation of energy along a ray tube in geometrical optics. This factor perhaps surprisingly predicts the correct phase change of $\pi/2$ when a ray passes through the caustic at $\sigma = -\gamma$; however, it incorrectly gives an infinite field at the caustic, thereby reflecting the characteristic failure of ray optical theories at focal surfaces. In order to overcome this difficulty, the field in the neighbourhood of the caustic should be written as a superposition of plane waves

$$u(\mathbf{y}) = \int_{\text{edge}} z(\sigma, s) \exp[ik\phi(\sigma, s)]\, ds \tag{5}$$

This integral around the diffracting edge is the starting point for the theory of Kravstov (1964) and Ludwig (1966), who derive expressions for u which are uniformly valid for a diffracted field containing a smooth caustic.

B. Geometrical Relationship Between Caustic and Defect

We can now derive the simple relationship between caustic and defect. For large k, the diffraction integral in eqn (5) can be evaluated by the stationary phase method, which states that the dominant contributions to $u(\mathbf{y})$ come from points on the edge where the derivative $\phi_s = 0$. For a point distant $R = |\mathbf{R}(s)|$ from the edge at s in the direction $\hat{\mathbf{R}} = \mathbf{R}/R$ (Fig. 1), $\phi_0(s) = R$ and it follows from eqn (3) that diffracted rays occur when

$$\phi_s(\sigma, s) = \cos\beta(s) - \hat{\boldsymbol{\sigma}} \cdot \mathbf{t} = 0 \tag{6}$$

Here $\hat{\boldsymbol{\sigma}} = \boldsymbol{\sigma}/\sigma$ and $\beta(s)$ is the angle between $\mathbf{R}(s)$ and the tangent $\mathbf{t}$ to the edge at s. Equation (6) reproduces the cones of diffracted rays which as we have seen, Keller predicted by extending Fermat's principle. The envelope of these rays, that forms the caustic surface for rays diffracted once by the edge, satisfies eqn (6) and also the equation $\phi_{ss} = 0$, which corresponds to the coalescence of two stationary phase points along the edge. This gives, for a ray to lie on the

caustic surface distant σ from the edge, the following equation for σ:

$$\sigma \frac{\partial \cos\beta}{\partial s} + \sin^2\beta - \boldsymbol{\sigma}\cdot\mathbf{n}\,\rho = 0 \tag{7}$$

where $\mathbf{n}$ is the principal normal and ρ is the radius of curvature of the edge at s.

Equations (6) and (7) actually hold for any incident wave field for which there is only one incident ray direction at each edge point $\mathbf{x}(s)$. For the point source, $\partial \cos\beta/\partial s$ is

$$\frac{\partial \cos\beta}{\partial s} = \frac{\sin^2\beta}{R} + \frac{\hat{\mathbf{R}}\cdot\mathbf{n}}{\rho} \tag{8}$$

The term $\sin^2\beta/R$ describes the influence of the curvature of the incident wavefront on the caustic geometry. Using eqns (7) and (8), the distance γ along the diffracted ray from the edge to the caustic is

$$\gamma = \rho\sin^2\beta\left[(\boldsymbol{\sigma}-\mathbf{R})\cdot\mathbf{n} - \frac{\rho\sin^2\beta}{R}\right]$$

For a plane wave incident in the direction $\mathbf{i}$, $R \to \infty$ so that $\partial \cos\beta/\partial s \to \mathbf{i}\cdot\mathbf{n}/\rho$ and $\gamma \to \rho\sin^2\beta\,(\boldsymbol{\sigma}-\mathbf{i})\cdot\mathbf{n}$. There will also be caustics formed by rays diffracted more than once by the edge, but they will be neglected here because their intensity is of lower order in k (Keller, 1957), and particularly because they do not generally occur in the same region of the scattered field as the caustic of the singly diffracted rays. An additional reason for neglecting multiple scattering will become clear in Section II.C.

In the far field for an incident plane wave, eqns (6) and (7) (which describe the caustic surface) reduce to those defining the caustic surface produced by the projection of the object in the incident beam direction. This property is important for our inversion procedure, so a proof is given in the Appendix. Denoting the parameters of this projection by a dash, the far field caustic is then defined by

$$\boldsymbol{\sigma}\cdot\mathbf{t}' = 0 \tag{9}$$

$$\boldsymbol{\sigma}\cdot\mathbf{n}' = \rho' \tag{10}$$

Equation (10) shows that the far-field caustic of singly diffracted rays contains the evolute of the projection of the edge, that is the locus of the centres of curvature of points on this projection. Equation (9) shows that the far-field caustic surface is a cylinder with generators in the incident beam direction, so that, in the classical limit $k \to \infty$ for which these interpretations hold, all far-field cross-sections are identical. These properties, which have been stated by Keller (1957) and observed optically by Coulson and Becknell (1922) are central to the present paper: if the geometry of the far-field caustic can be observed in ultrasonics, the shape and in some cases the size of the defect

projection in the incident beam direction of a crack-like object can be derived simply by constructing the involute of the caustic. The extent to which this involution can give a unique result will be discussed in Section III. The position of this classical caustic does not change with wavelength (though Section IV below shows that its height and width do change); therefore, caustics can be observed with broadband, pulsed ultrasound as well as with continuous waves.

Cusps correspond to the coalescence of three geometrical ray paths, or three stationary phase points on the projection of the edge, which occurs when $\phi_{s's's'} = 0$. Differentiating eqn (10), this gives

$$\sigma' \cdot \mathbf{n}'_{s'} - \mathbf{x}'_{s'} \cdot \mathbf{n}' = \rho'_{s'} \tag{11}$$

Using the Frenet formulae (e.g. Mathews and Walker, 1964), $\mathbf{x}'_{s'} = \mathbf{t}'$ and $\mathbf{n}'_{s'} = -\mathbf{t}'/\rho'$, the latter equation resulting because the projection of the edge is planar by definition, so its torsion is zero. Combining these results with equations (9) and (11), it follows that $\rho'_{s'} = 0$ for cusps in the far-field caustic, i.e. cusps occur when the curvature or radius of curvature of the corresponding point on the projected edge is extremal, as is generally true for the evolutes of plane curves (e.g. Courant and John, 1965). Also, the cusp is normal to the tangent at this corresponding extremal point. The importance of these properties of cusps for the geometrical inversion of scattered fields will be discussed in Section III.

In the near field of the object, we must return to eqns (6) and (7) for the description of the caustic surface. Cusp lines satisfy in addition the equation $\phi_{sss} = 0$; calculating this from eqn (7), no simple correlation results between cusps and distinctive geometrical features of the object, as occurs for the far field. For this reason, the far field appears more useful for simple inversion. An exception to this is the case of normal incidence on a planar object, for which the edge is trivially equivalent to its projection and the cross-section of the caustic surface is the same at any distance from the object. Unfortunately, it appears from the discussion in Section IV that the caustic will be more difficult to observe experimentally in the far field than in the near field.

For the elastic wave case, two families of cones of singly diffracted rays occur, the second as a result of mode conversion (Achenbach and Gautesen, 1976). These families are related by Snell's law, and apart from the case of normal incidence on a planar crack, two spatially separated caustic surfaces result. For example, the diffraction of a P-wave incident at $\beta_p(s)$ on the edge yields a P-wave caustic surface whose geometry is equivalent to that described by the scalar wave theory, together with an S-wave caustic. The geometry of this S-wave caustic is identical with that predicted in scalar wave theory for rays incident at the various points s on the edge at angles $\cos^{-1}[(v_s/v_p)\cos\beta_p(s)]$, where v_p and v_s are the respective wave speeds. When

$\beta_p(s)$ is significantly different from $\pi/2$, this S-wave caustic causes no complication in far-field experiments because it is well separated from the P-wave caustic. Of course, the two caustics touch for points on the edge where $\beta_p(s) = \pi/2$, but general properties of the caustic geometry derived from catastrophe theory, as discussed below, should avoid any confusion between them. In addition, S-waves can be reduced or eliminated experimentally by, for example, using as detectors normal probes with low sensitivity to S-waves, or for pulsed ultrasound, by separation in the time domain. For these reasons, a detailed analysis of caustics in elastodynamics is not essential for the present work.

C. *Possible Shapes of Caustic Sections Using Catastrophe Theory*

Any theoretical limitations that can be placed on the possible shapes of the caustics would greatly assist their identification. For this purpose, we use and extend the application of the catastrophe theory of Thom (1975) to wave phenomena (Berry, 1976; Poston and Stewart, 1978). This theory is concerned with the typical local geometry of functions, in the present case those describing the caustic pattern. In the far field, this pattern depends on two coordinates (those of the diffracted field at infinity), as well as on the shape and size of the diffracting edge. While the *global* description of this edge requires two parameters, only one—the projected edge parameter s'—is needed for its local description. The other parameter (say, a polar angle) will influence the global topology of the caustic surface, but will determine only the orientation of local singularities. not their form or type. In the language of catastrophe theory, the caustic pattern then depends on just one internal parameter, so the rank is one and only cuspoid catastrophes can occur. Also, the two dimensions of the far field imply that the co-dimension of the caustic pattern in that region is two, so that only the fold catastrophe, which appears as ordinary points on the caustic surface, and cusps, are generically ("typically") possible. Since in addition "open-ended" folds are not permitted, any normal section through the far-field caustic surface produced by scattering from a purely convex edge projection typically consists of a continuous closed line interrupted only by cusps. This can be taken as a rule to help distinguish caustics from other structure in the diffracted field.

This insight into caustic geometry provides an additional protection against complications due to caustics of multiply-scattered rays: in following the line of a supposed singly-scattered caustic section, crossing to any other accidentally intersecting caustic would be avoided, since this crossing would result in a forbidden local topology. Since experiments are of course carried out at finite λ, the caustic is not infinitely sharp. but is spread by characteristic functions called "diffraction catastrophes", which clothe the diffracted field in the

neighbourhood of the caustic by interference of the near-coalescing rays. This caustic width is important in considering the experimental viability of the inversion technique, and will be discussed in Section IV for the Airy function-like spreading of the fold catastrophe. In addition, the peak intensity in the diffraction catastrophes does not occur exactly at the desired position of the classical caustic, but is slightly displaced towards the bright side as described by an Airy function for the fold, and by Pearcey (1946) for the cusp. The correction of an observed caustic for this shift only requires a knowledge of the frequency spectrum; its importance will be investigated in a future study.

Non-generic caustics, which may be structurally unstable sections of higher catastrophes, can occur as a result of symmetry or by accident. However, with few exceptions such as the field scattered by a spherical void, they are unlikely to be important for our ultimate objective of studying real defects in solids. Berry (1976) has given some discussion of these non-generic cases, which are perhaps more easily pictured for catastrophes of rank two. Complications arise if the edge projection contains points of inflection, since the caustic then extends laterally to infinity, and appears to be discontinuous. These caustics would not be observed in full, so the discussion of this section excludes edge projections with concave parts; one example will be considered in Section III.

A near-field experiment involves an additional dimension in comparison to the far field, so that the co-dimension in this case is three. Therefore the next cuspoid catastrophe can occur at those singular points along the cusp lines which satisfy $\phi_{ssss} = 0$. Clear examples of these so-called "swallowtail" catastrophes have been observed in the optical case (Berry, 1976); however, experimental limitations discussed in Section IV may render difficult the observation in ultrasonics of the compressed form of their near singular sections.

III. Geometrical Inversion Procedure

The caustic pattern is always centred in the geometrical shadow of the defect, and often lies completely within this shadow. In this section, we explain how the geometry of the caustic section can yield the shape and size of the defect. We firstly consider two approaches to the simple but important case of a crack whose projection in the direction of an incident plane wave is an ellipse. A discussion is given of some distorted elliptical shapes; these illustrate the central role played by cusps in the caustic. In part B, inversion for more general shapes is described.

A. The Elliptical Crack

Consider a diffracting edge whose projection is an ellipse with principal axes of length $2a$ and $2b$. Then the cross-section of the far-field caustic will be the

evolute shown in Fig. 2, which is an astroid (e.g. Courant and John, 1965). Conversely, when the caustic is observed to be an astroid, it is immediately known that the edge projection is elliptical. If the distances between the two pairs of opposite cusps are measured as $2\xi_0$ and $2\eta_0$, it follows from the

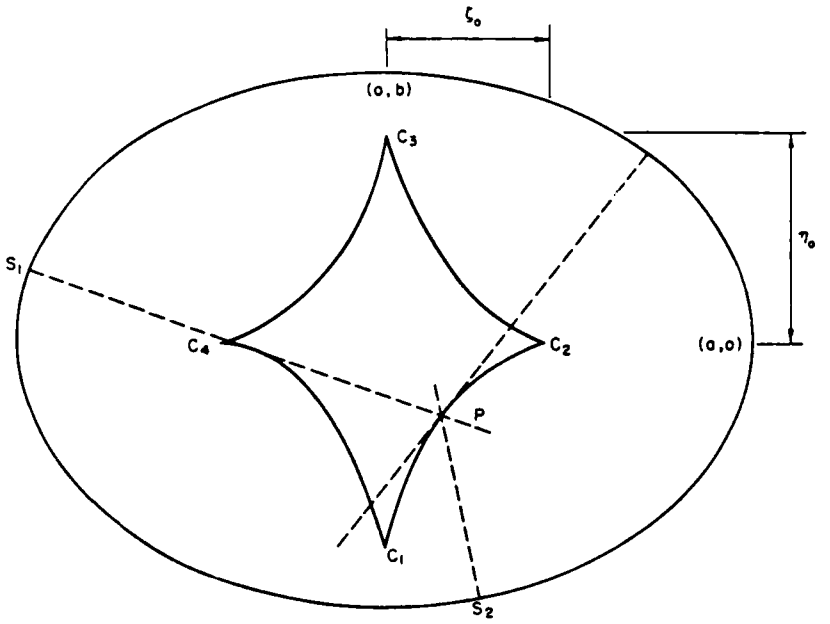

FIG. 2. An elliptical diffracting edge and the corresponding far-field caustic. This and Figs 3 and 4 are superpositions of the spaces of the edge projection and of the far-field diffraction pattern, drawn on the same scale. The two cusps lying along the major axis are always inside the geometrical shadow; the other two cusps are outside the shadow for ellipses having eccentricity $> 1/\sqrt{2}$. The broken lines indicate all rays contributing to the field at point P, as discussed in Section IV.A.

equation of the astroid $(a\xi_0)^{2/3}+(b\eta_0)^{2/3} = (a^2-b^2)^{2/3}$ that the major axis of the ellipse is $2a = -2\xi_0\eta_0^2(\xi_0^2-\eta_0^2)^{-1}$, and $b/a = \xi_0/\eta_0$. Since the cusps are normal to the tangents at the corresponding extremal points on the edge, the ellipse is oriented as shown in Fig. 2 with its major axis parallel to the line $2\xi_0$ between the closer pair of cusps. Thus it is actually not necessary to observe the complete caustic in this simple case—only the positions of cusps in the rectangular array are required.

It is useful to construct the involute of the astroid in another way, based on the knowledge that the caustic is the locus of centres of curvature of the edge. Imagine a string set along the inside of the section C_1C_2 of the astroid (Fig. 2) and extending beyond C_2 in the direction of the cusp by a distance equal to the

minimum radius of curvatures of the ellipse, which is known from the caustic to be $b^2/a = \xi_0^3(\eta_0^2 - \xi_0^2)^{-1}$. Unwinding this string traces out the first quadrant of the ellipse. Next, wind the string on to the section $C_1 C_4$ of the astroid to produce the second quadrant of the ellipse. Proceeding clockwise around the astroid and alternately winding and unwinding in this way, the complete ellipse is generated in an anticlockwise sense. This procedure also demonstrates that the arc length of the caustic between neighbouring cusps is the difference in the corresponding extremal radii of curvature.

Some special cases of the ellipse are of interest. For eccentricity $\varepsilon \to 1$, $\xi_0 \to a$ so that $\eta_0 \to \infty$, i.e. one pair of cusps extends laterally to infinity and is not observed. Therefore, tilting the object about the axis of the closer pair of cusps enables direct measurement of the major axis, since the two remaining cusps become coincident with the ends of the narrow shadow boundary. Also, for $\varepsilon \to 0$, the edge approaches a circle and $\xi_0 \simeq \eta_0 \to 0$. Therefore, for ellipses of low eccentricity, the four cusps form an approximately square array which will be too small to resolve. Ultimately, for the circle $\varepsilon = 0$ and the cross-section of the caustic pattern degenerates to a single point, which is well known in optics to have an intensity comparable to that of the incident field (e.g. Born and Wolf, 1959). Observation of such a degenerate caustic immediately gives the projection of the diffracting edge as being circular. This particular case is not described in the classification given by Thom's theorem because of its high symmetry. The size of a nearly circular defect may be found by tilting the specimen, giving an elliptical projection whose caustic is an astroid of convenient dimensions.

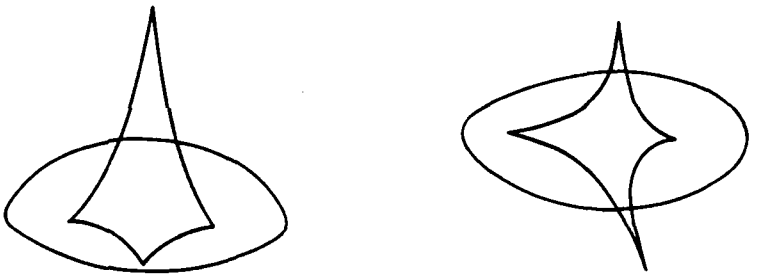

FIG. 3. Distorted ellipses with their corresponding caustics. (Left) One side of the ellipse more eccentric than the other. (Right) One minimum of curvature shifted from the symmetrical position.

Some other examples of caustic/diffracting edge pairs can be generated from the elliptical case. If one side of a distorted ellipse is flatter than the other, a caustic will result which has the two pairs of cusps arrayed at right angles, but not symmetrically (Fig. 3, left). Again, if an ellipse is distorted by shifting one turning point from the symmetrical position, the cusps will no longer be

directed as two opposing pairs at right angles (Fig. 3, right). Nevertheless, the directions of the tangents at the turning points are immediately known by inspection of the caustic.

If the edge projection contains a concave part, the caustic will appear discontinuous, since it extends to infinity at points of inflection. Figure 4 shows an ellipse "pressed in" at one end, and the corresponding caustic. Note that the

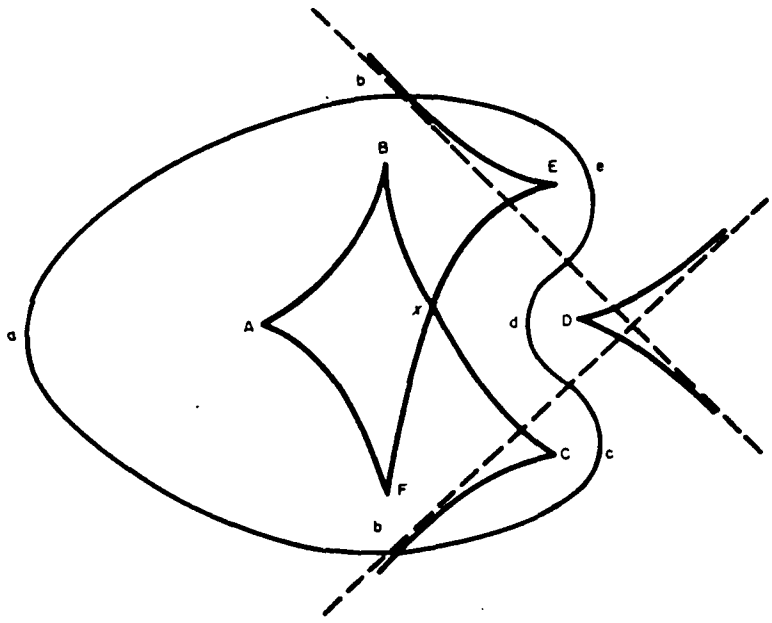

FIG. 4. An ellipse "pressed in" at one end, and its corresponding caustic. The association between cusps and turning points is indicated by letters. The pattern in the region marked X is a superposition of elementary fold catastrophes, and should not be mistaken for a section of some higher catastrophe.

intensity of the caustic tends to zero far out along those sections which are asymptotic to the normal at the points of inflection, because the density of contributing ray paths then approaches zero. Therefore, only a limited part of the caustic will actually be observed. A less severe depression in the end of the ellipse will produce the cusp marked D further away from the rest of the caustic. A "flattened end" on an ellipse which is nevertheless convex will give a caustic section as a closed line containing six cusps. Three of these cusps coalesce into one as the distortion of the ellipse is reduced to zero, again producing the simple four-cusped astroid.

B. General Convex Crack

Any smooth, purely convex closed shape has an even number of turning points, since maxima and minima of curvature must alternate in circuit. Therefore, there is an even number of cusps in the caustic which is itself a partial check on an experiment. The diffracting edge projection is normal to cusps at the points of extremal curvature, so the orientation of the projection is known by inspection of the cusps. Edge projections corresponding to caustics of four, six, eight or higher even numbers of cusps can be constructed by alternately folding and unfolding each caustic section in turn, just as was done for the ellipse. For this general case, there is no representation of the caustic in terms of elementary functions as there was for the astroid. Therefore, the radius of curvature at one extremal point cannot be deduced simply from the spacing of cusps, and a different method must be sought to achieve a unique reconstruction.

Since the cusps corresponding to the minima of $\rho(s)$ are less sharp than those corresponding to maxima (e.g. see the ellipse of Fig. 2), it should be possible to identify at least one cusp corresponding to a minimum of $\rho(s)$, say ρ_1. Beginning with this cusp, and assuming particular values for ρ_1, a one-parameter family of possible involutes of the caustic can be generated. It then remains to choose the correct involute from this set. One technique suitable for some cases of planar defects would be to tilt the object about an axis between two approximately opposite cusps, whose spacing would then be asymptotic to the length of the narrow shadow boundary. This procedure enables direct measurement of one length in the diffracting edge, which is sufficient to select the correct involute. The question remains, however, whether the cusps can be identified for the highly tilted edge, since the high frequency approximation at the root of our procedure becomes less valid as the radii of curvature at the ends of the narrow projection become small. If one length in the edge can be determined by a different technique, as is possible for some objects using ultrasonic spectroscopy (e.g. Bifulco and Sachse, 1975; Adler *et al.*, 1977), the desired involute can again be chosen from the set of possibilities.

Involuting the far-field caustic gives the projection of the diffracting edge in the incident beam direction. The orientation of a planar defect in three dimensions could be inferred from several such measurements involving different projections. Another approach is to examine the variation of the caustic pattern as the plane of observation is moved into the near field: the special case of normal incidence produces no change of the caustic in this region. Identifying this behaviour defines the normal to a planar defect. The extent to which the three-dimensional structure of non-coplanar diffracting edges can be found is not considered here, both because of its greater complexity and because most practical applications of defect sizing in ultrasonics do not require this detail.

IV. Experimental Work

We have seen where in the diffracted field to look for caustics, and discussed their possible shapes. Before proceeding with experiments, it is desirable to have some idea of the sensitivity and resolution needed. These questions are addressed in part A. In part B, our preliminary observations of ultrasonic caustics are presented.

A. Anticipated Caustic Contrast

The ease of observation of caustics in ultrasonics will depend on their width as well as their intensity relative to the background in their neighbourhood. These properties will be studied by considering a particular but typical case, specifically normal incidence of a plane wavefront on a planar elliptical crack, described parametrically by $x = a\cos\theta$, $y = b\sin\theta$. Calculations will be made for a point on the caustic which lies within the geometrical shadow of the ellipse; the contrast will be low for any part of the caustic which lies outside this shadow in the bright field of the incident wave.

Referring again to Fig. 2, we see that the coalescence of two stationary phase points at $\theta = \pi/4$, for example, contributes to the caustic surface along a line which projects into the astroid segment $C_1 C_2$ at point P. In addition, these rays from $\theta = \pi/4$ contribute as from an isolated stationary point to caustic segments in the first and third quadrants, respectively before and after passing through the caustic. Equivalently, there are two "isolated" contributions from the fourth and second quadrants to the field at all points along the caustic line through P. The question then reduces to a comparison between the intensity on the "bright side" of the caustic (the inside of the astroid), to which four rays contribute including two which coalesce, and the intensity on the "dark side" to which two rays contribute.

For the planar crack specified, the function $z(\sigma, s)$ in the diffraction integral (eqn (5)) is proportional to σ^{-1}. If the constant of proportionality, which depends on the amplitude of the incident wave, is set equal to unity, the intensity u_I^2 scattered to a point y in the far field from an isolated stationary point s_I is (adapting, for example, Skudrzyk, 1971)

$$u_I^2(\mathbf{y}) = 2\pi[k\sigma^2\,\phi_{ss}(s_I)]^{-1} \tag{12}$$

For two stationary points coalescing at s_c, $\phi_{ss} \to 0$ and (12) should be replaced by the transitional approximation

$$u_c^2(\mathbf{y}) = \frac{4\pi^2}{\sigma^2}\left(\frac{2}{k\phi_{sss}(s_c)}\right)^{2/3} Ai^2(-\delta) \tag{13}$$

where the argument of the Airy integral is given near the caustic (Ludwig,

1966) by

$$\delta = (2k^2/|\alpha|)^{1/3} d \tag{14}$$

In eqn (14), α is the radius of curvature of the caustic and d is the perpendicular distance from the field point $\mathbf{y}$ to the caustic. Using eqns (3) and (6), the remaining functions in eqns (12) and (13) are found to be

$$\phi_{ss}(s_1) = (1 - \boldsymbol{\sigma} \cdot \mathbf{n}/\rho)/\sigma \tag{15}$$

$$\phi_{sss}(s_c) = \rho_s/\sigma\rho \tag{16}$$

For the far field, σ can now be replaced by the distance z_0 between the diffracting object and the plane of observation of the caustic section.

The intensity on the dark side of the caustic is found by summing incoherently the contributions from the appropriate isolated edge points, s_1 and s_2. This procedure ignores any interference between these two rays; any resulting intensity variation would in any case be smoothed by an experiment using a broadband transducer. On the bright side of the caustic, the maximum intensity is the sum of these two rays plus the maximum value of the caustic field, which occurs at $\delta = 1{\cdot}02$. The parameters ρ and ρ_s for the edge, α for the caustic and $\boldsymbol{\sigma} \cdot \mathbf{n}$ for the edge points s_1 and s_2 are found by Doyle (1980, Appendix I) for the elliptical crack for $\theta = \pi/4$ and its corresponding caustic along the line through P. Table I lists the maximum contrast

$$C_{max} = \frac{u_{C_{max}}^2 + (u_1^2 + u_2^2)}{(u_1^2 + u_2^2)}$$

at the caustic section 100 mm behind the plane of the ellipse $(a, b) = (10, 7{\cdot}5)$ mm for 10 MHz in water and typical P and S wavelengths in

TABLE 1

Intensity Changes and Widths for Caustics

	Water	Steel (S)	Steel (P)
λ(mm)	0·15	0·30	0·60
C_{max}	3·12	2·68	2·32
(dB)	(4·94)	(4·28)	(3·65)
C_{av}	2·02	1·79	1·64
(dB)	(3·04)	(2·56)	(2·14)
α_w(mm)	0·24	0·37	0·60

The intensity changes across the caustic, at the point P defined in the text, are expressed as a ratio and in *dB*. Calculations are for 10 MHz for the section 100 mm behind an elliptical crack having semi-major axes $(a, b) = (10, 7{\cdot}5)$mm.

steel. The calculated changes in intensity level of the order of 3·5–5 dB can easily be observed experimentally. In addition, Table I gives estimates of the contrast C_{av} predicted if $Ai^2(-\delta)$ is averaged over its first two fringes; the changes of intensity level of about 2–3 dB are also observable.

Examination of eqns (12)–(16) shows that the intensity contributed by isolated edge points decreases as σ^{-1} for large σ, which is expected since each point on the edge scatters as an infinitesimal section of an infinite half-plane, which gives a cylindrical wave. The caustic intensity decreases more rapidly, as $\sigma^{-4/3}$. The contrast at the far-field caustic therefore decreases weakly as $\sigma^{-1/3}$, so the choice for σ (that is, z_0) is not critical from this theoretical viewpoint. Practical limitations of transducers are more important for choosing z_0, since the lateral smearing of a caustic, produced by the finite spread of waves incident on the edge, increases proportional to z_0. Equations (12) and (13) also show that the values for C increase only as $k^{1/3}$, so a reasonable estimate of C in an experiment is found by taking k to correspond to the centre frequency of the transducer; it is not necessary to integrate over the spectrum, though this could readily be done.

An estimate of the width of the caustic is the distance d_w from the maximum intensity on the bright side to the position on the dark side where u_C^2 has dropped to 10% of its maximum value. Equations (13) and (14) then give

$$d_w = 1{\cdot}8(|\alpha|/2k^2)^{1/3} \tag{17}$$

The values of d_w in Table I are of the order of the corresponding wavelength λ, or slightly greater. Since λ is also a rough estimate of the resolution that can be achieved in any detection system which may be used to measure the field, it is clear that the inherent width of the contrast due to caustics should not prevent their observation. This conclusion becomes gradually less valid as $|\alpha|$ increases, such as for the part of the caustic corresponding to edge points near the minor axis of a highly eccentric ellipse. Since d_w decreases as $k^{-2/3}$, higher frequencies (say 10–20 MHz for ultrasonic NDE) produce sharper caustics.

The spacing of the Airy fringes in ultrasonics, given at least roughly by equations similar to equation (17), are of the order of the wavelength, so these fringes will not readily be observed. This is part of the reason why caustics have been ignored in ultrasonics, whereas in the optical case $|\alpha| \gg \lambda$ so the fringe spacings are also much greater than λ, allowing easy observation.

If the incident wavefront is curved, as for example from a point source, the interpretation of the caustic is more complicated because its geometry depends on the curvature of the incident wave as well as on that of the edge. Nevertheless, the caustic is just as sharp and easily detected. The most important factor experimentally is to tailor the incident wave to minimize the angular spread of wavelets incident on a single point on the edge, since this spread smears out the caustic. This smearing is likely to remove any remnants

of the Airy fringes, so the values for C_{av} in Table I give a more realistic estimate of the expected caustic contrast than those for C_{max}.

We conclude from these calculations that ultrasonic caustics should be observable in carefully designed experiments. Our preliminary observations will now be discussed.

B. Preliminary Observations

1. *Experimental Goals*

Preliminary experiments have been carried out to investigate the shadow region of circular and elliptical defects. The experiments may be divided into two complementary areas of investigation. First, circular and elliptical disks in water were used to demonstrate some of the essential features of the diffraction field. Second, the shadow region of defects in diffusion bonded titanium were briefly considered in order to verify the potential usefulness of these techniques in nondestructive evaluation.

2. *Diffraction by Circular and Elliptical Disks in Water*

Both circular and elliptical disks were used as diffracting objects. The circular disk was constructed of two thin quartz disks (Fig. 5) which were cemented to a rubber O-ring. The diameter of the quartz disk was 2·54 cm. A small brass rod with a diameter of 1·6 mm was attached to one side of the structure in order to provide support. The essential feature of this composite structure was the air gap in the middle which blocked transmission of ultrasound into the shadow region.

The elliptical diffraction disk (Figs 6 and 7) was constructed from two identical ellipses separated by a spacer. The ellipses and spacer were cut from an aluminium sheet having a thickness of 0·58 mm. The spacer placed between the two ellipses provided an air gap. The composite structure was held together with waterproof cement. The edges of the structure were machined to form a sharp edge around the periphery. A small stainless steel rod having a diameter of 0·3 mm was attached to one side of the structure for support. The length of the major axis was 2·54 cm and the length of the minor axis was 2·08 cm.

Bragg imaging was the initial technique employed to investigate the diffraction field. A 5 cm square quartz transducer was driven by a CW exciter at frequencies of 14 MHz and 18 MHz. The circular diffracting disk was placed in front of the transducer and oriented to provide either a circular or projected elliptical defect. A Bragg imaging system similar to the one described by Korpel (Korpel, 1968; Martin, Adler, and Breazeale, 1972) was used to image a cross-section of the shadow region behind the defect. The circular disk was

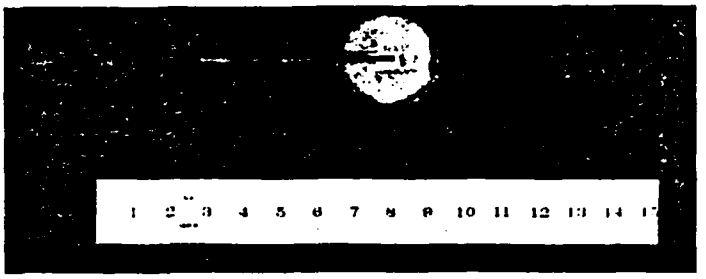

FIG. 5. Photograph of circular quartz disk.

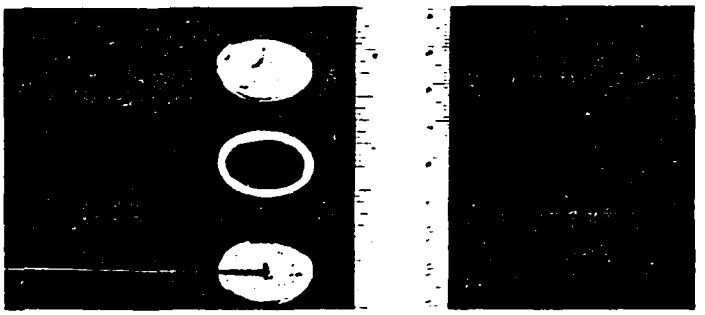

FIG. 6. Photograph of disassembled metal ellipse.

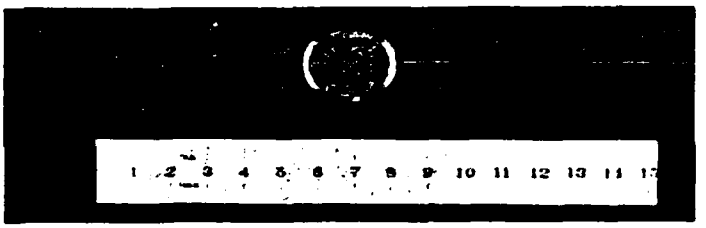

FIG. 7. Photograph of assembled metal ellipse.

rotated through an angle of 35° in order to provide a projected elliptical defect. A typical image obtained with the Bragg system is shown in Fig. 8. The image of the shadow region appears as a dark spot in the center of the bright Bragg diffraction order. The diffraction field from the disk appears as the bright structure within the shadow region. The conclusion based upon this photograph and similar photographs is that Bragg imaging techniques performed with a Bragg system having typical imaging capabilities provide a somewhat qualitative indication of some structure within the shadow region; however, the results are not easily repeated or quantitative in nature.

FIG. 8. Bragg image of diffraction field behind 1-inch circular disk tilted through an angle of 35° (frequency 14 MHz).

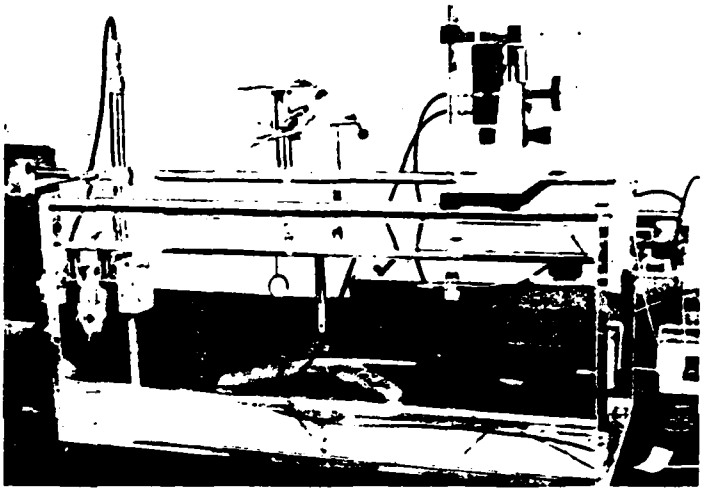

FIG. 9. Photograph of hydrophone, tank, transducer, and circular disk.

In order to obtain quantitative information, the shadow region was scanned with a miniature hydrophone (Fig. 9). The active receiving element of the probe consisted of a piezoelectric disk with a diameter of 250 μm. Electronic buffering and amplification were built into the body of the hydrophone in order to maintain a good signal-to-noise ratio and a flat frequency response. The receiving element of the probe was mounted at the apex of a cone with an acoustically absorptive center. This design, along with the small size of the sensing element, minimized the interference by the probe with the acoustic field. A micromanipulator mounted on the observation tank permitted

precision movements of the hydrophone to be made along three mutually perpendicular axes. The position of the hydrophone was read to within 0·1 mm by means of vernier scales. The output from the hydrophone was read from the peak to peak signal on an oscilloscope connected to the hydrophone preamplifier. The transducer used in this phase of the investigation was a 5 cm quartz transducer with a resonant frequency of 2 MHz. It was driven at the odd harmonics by means of a pulsed exciter. Either the tilted disk or the plane ellipse was placed in front of the transducer and the probe was scanned across the geometrical shadow region behind the disk.

Figure 10 indicates the diffraction field in the shadow region of the circular disk oriented normally to the acoustic field. The frequency was 2 MHz and the

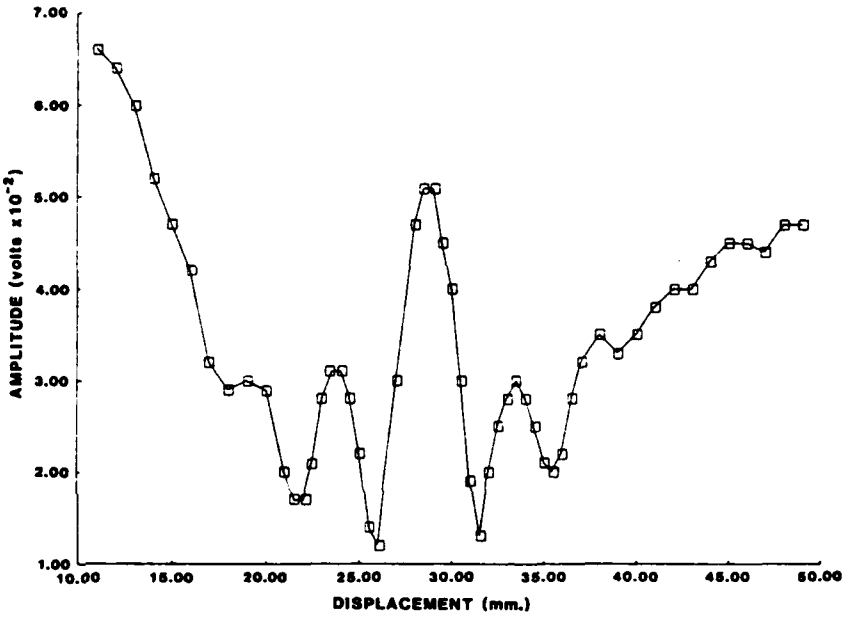

FIG. 10. Vertical scan along diameter of 1-inch circular diffraction disk at normal incidence. The Arago spot is evident in the centre of the pattern. Fresnel fringes are concentrically located about the centre (frequency: 2·25 MHz, probe distance, 14·5 cm).

probe was scanned along the vertical diameter of the disk. The pattern indicates the presence of the Arago spot in the center which is "clothed" by the Fresnel fringes that are located concentrically about the center.

The diffraction field for the planar aluminium ellipse is indicated in Figs 11 and 12. Figure 11 corresponds to a vertical scan along the major axis and Fig. 12 corresponds to a horizontal scan along the minor axis. The probe, in each

case, was located at a distance of 24·1 cm from the defect. The two dominant peaks in each pattern indicate the possible existence of the cusps in the caustic pattern as shown graphically in Fig. 2. The separation of the cusps was calculated theoretically from the parametric equations for the astroid (Doyle, 1980). The theoretical separation is shown graphically in each figure by a horizontal arrow drawn above the diffraction pattern. The fact that the peaks of the experimental curves are in most cases inside the predicted theoretical separation is to be expected from the form of the diffraction catastrophe "clothing" the cusp (Pearcey, 1946). The asymmetries evident in the diffraction pattern are due to the variations in the acoustic field of the large transducer.

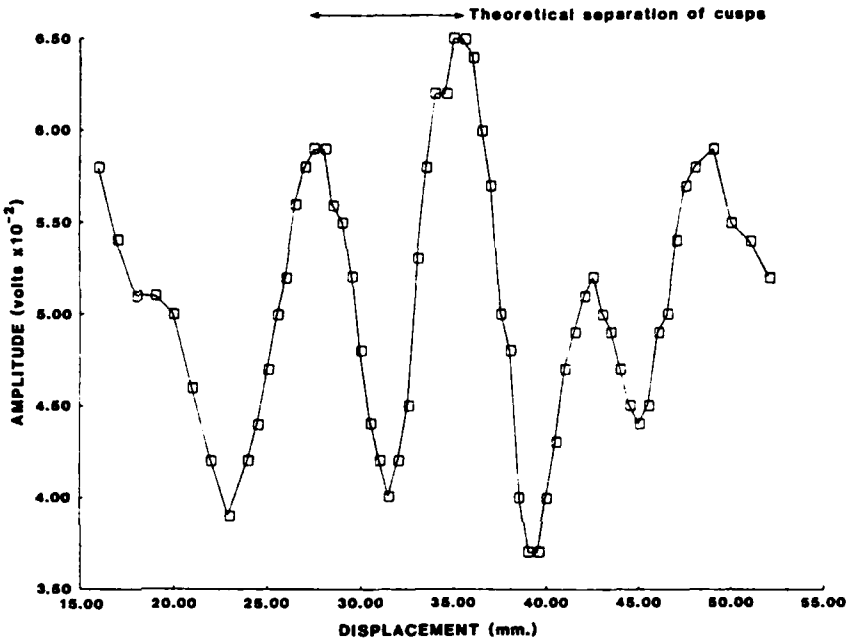

FIG. 11. Vertical scan along the major axis of the planar aluminum ellipse. The two peaks indicate the possible existence of cusps. The horizontal arrow graphically indicates the theoretical separation of the cusps (8·4 mm). The ultrasonic frequency was 1·89 MHz and the distance from the probe to the ellipse was 24·1 cm.

This assertion is based upon both the observation of similar asymmetries in the diffraction pattern for a circular disk at normal incidence and the presence of asymmetries in the beam profile of the transducer. These asymmetries in the acoustic field should only affect the relative amplitudes of the various components in the diffraction field and not the separation of the components.

The diffraction field for a 35° tilted circular disk is compared with an

equivalent plane ellipse in Figs 13 and 14. The probe distance in each instance was 16·5 cm from the diffracting disk. Disregarding the differences in relative amplitudes, the separation of the cusps is approximately the same. A comparison of similar diffraction patterns indicated that in most cases there is reasonable agreement between the diffraction patterns of the circular tilted disk and the planar ellipse

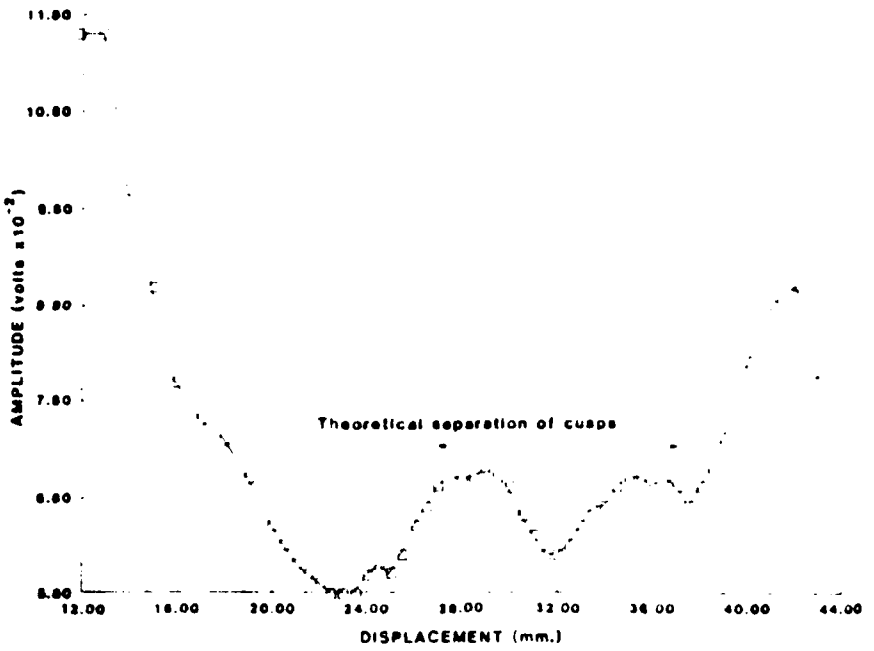

FIG. 12. Horizontal scan along the minor axis of the planar aluminium ellipse. The separation of the two peaks was compared with a theoretical prediction of 10·2 mm for the separation of the cusps. The frequency was 1·89 MHz and the distance from the probe to the ellipse was 24·1 cm

The behaviour of ordinary points in the caustic pattern was investigated (Fig. 15) experimentally. The 35° tilted disk was used in this area of the investigation. The probe was scanned along a line oriented at 45° relative to the minor axis of the projected ellipse. The two peaks in Fig. 14 indicate the possible existence of the two ordinary points in the caustic pattern. One of the ordinary points corresponds to point P in Fig. 2; the other ordinary point corresponds to a point located symmetrically between C_3 and C_4 in Fig. 2. A theoretical calculation was made for the separation of the ordinary points using the parametric equations for the asteroid (Doyle, 1980). This theoretical separation is indicated graphically by the horizontal line in Fig. 15.

3. *Defects in Metals*

The next phase of the investigation consisted of scanning the geometrical shadow region of a 5 mm penny-shaped crack located in the center of a diffusion bonded titanium disk having a diameter of 10 cm and a thickness of 2·5 cm. A ceramic transducer was driven in a pulsed mode with a frequency of

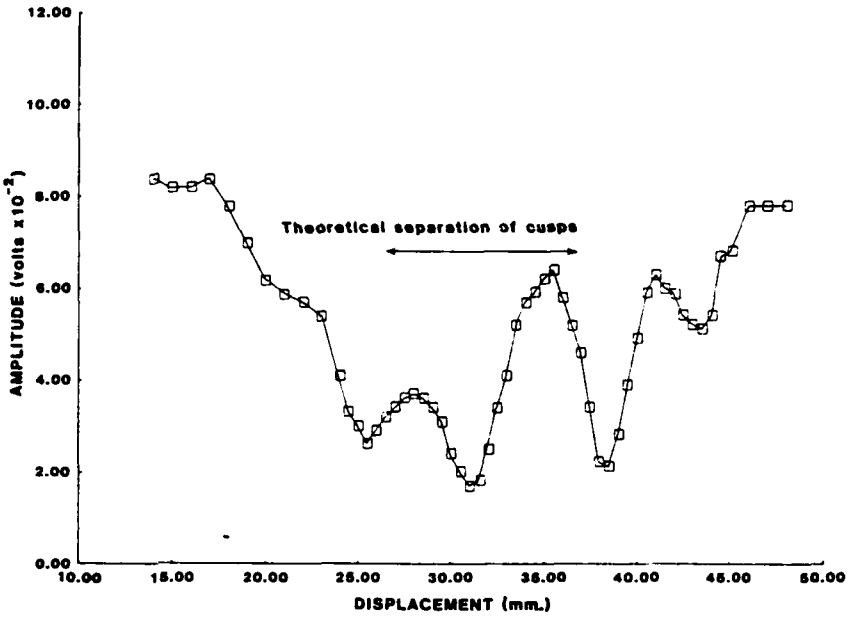

FIG. 13. Horizontal scan along the minor axis of the one-inch circular disk rotated through an angle of 35°. The separation of the peaks was compared with a theoretical prediction of 10·2 mm for the separation of the cusps. The frequency was 1·89 MHz and the distance from the probe to the ellipse was 16·5 cm.

6·3 MHz. The penny-shaped crack was oriented normally to the acoustic axis and the probe was located at a distance of 5·08 cm from the crack (Fig. 17). The scan through the shadow region is indicated in Fig. 16. The peak in the centre of the shadow region corresponds to the Arago spot.

4. *Conclusions Based upon Preliminary Observations*

The observations presented in this section are the preliminary phase of a long-range investigation; therefore, any conclusions are based upon somewhat limited data input.

A comparison of preliminary experimental observations and theoretical predictions indicate reasonable agreement in most areas considered at lower frequencies; there are indications of cusps and ordinary points. The separation of these points agree nominally well with the theoretical predictions. The separation of the cusps appears to remain fairly constant with increasing probe distance in accordance with theoretical prediction for incident plane

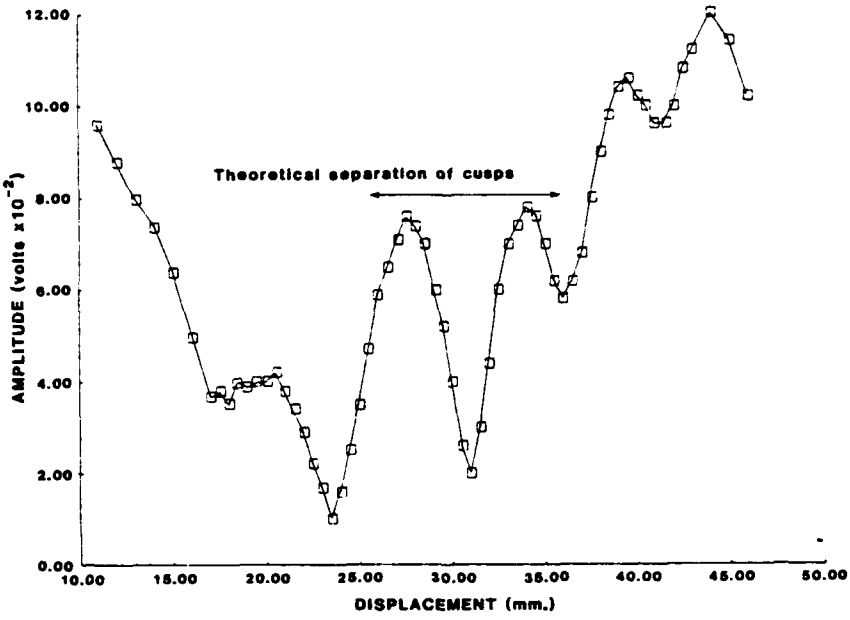

FIG. 14. Horizontal scan along the minor axis of the planar aluminum ellipse. The separation of the peaks was compared with a theoretical prediction of 10·2 mm for the separation of the cusps. The frequency was 1·89 MHz and the distance from the probe to the ellipse was 16·5 cm.

waves. In other areas, however, there appears to be some discrepancy between theory and experiment at higher eccentricities for the elliptical disk; the cusps along the minor axis do not appear to recede into the bright field as predicted by the theory. In addition, the width of the observed pattern is broader than the theoretical prediction for the width of the caustic. These considerations and other features such as the dominating presence of Fresnel diffraction fringes indicate the need for more experimental and theoretical work in this area. On the other hand, the feasibility of applying these techniques to defects in metals has been demonstrated and this indicates the possibility for applications to nondestructive evaluation.

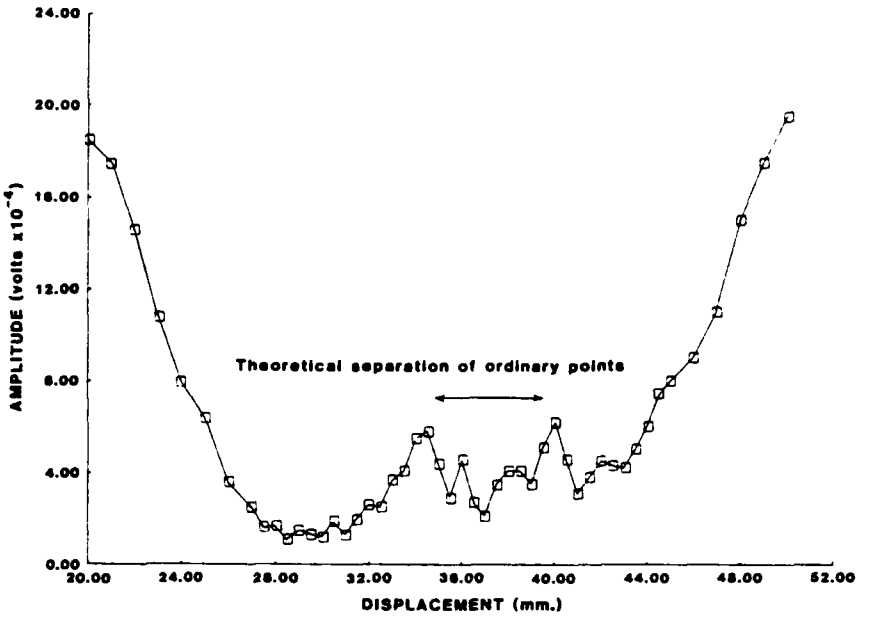

FIG. 15. Scan along a line oriented at 45° relative to the minor axis of the ellipse projected by the 1-inch circular disk tilted through an angle of 35°. The separation of the peaks was compared with a theoretical prediction of 4·7 mm for the separation of the ordinary points. The ultrasonic frequency was 14 MHz and the distance from the probe to the disk was 25·4 cm.

V. DISCUSSION

A. Caustics from Voids and Inclusions

To date, this article has dealt with diffraction caustics from crack-like defects. In this subsection, we digress briefly to compare the topology of caustics formed by scattering from voids and inclusions.

In the near field of the rays transmitted by a solid or liquid-filled inclusion, caustic sections described as elliptic or hyperbolic umbilics are expected, though likely to be masked by diffraction effects and experimental smearing. These catastrophes of rank two are possible because two parameters are needed for the local description of the defect, compared with one parameter (s) for the crack. In the far field, the co-dimension is two and again only elementary folds and cusps are generically possible, therefore the topology of far-field caustics cannot distinguish between inclusions and planar defects. This result does not hold if the orientation of the specimen is regarded as an additional accessible control parameter in the sense discussed by Berry (1976); then, singular umbilic sections can in principle be generated in the far field by

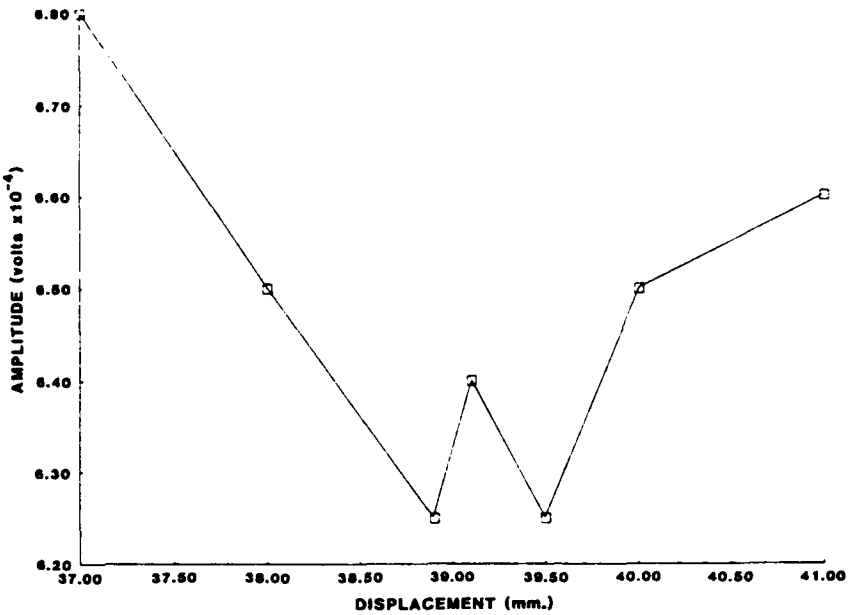

FIG. 16. Vertical scan through the shadow region of a 5 mm penny-shaped crack located in the centre of a diffusion bonded titanium disk having a diameter of 10 cm and a thickness of 2·5 cm. The disk was oriented normally to the ultrasonic beam. The Arago spot is evident in the centre of the diffraction pattern. The ultrasonic frequency 6·3 MHz and the probe was located a distance of 5·08 cm from the defect.

rotating the specimen. Nye (1978) has carried out a detailed study of caustics of rank two for an analogous case of light passing through water droplet lenses.

For voids, umbilic sections are possible in the near field, because the local description of the source of bulk waves produced by decay of the creeping waves requires two parameters (such as (s) plus arc length along the geodesic). However, just as for the scattering by inclusions, these umbilics are not likely to be readily observable. The far field again consists only of elementary folds and cusps. An important singular case is the spherical void, which gives a point caustic at the center of its shadow for all orientations. This case is not described by Thom's theorem because of its symmetry.

B. Comparison with Other Inversion Procedures

It is not possible at present to state the lowest l/λ value for which the diffracted field can be meaningfully interpreted in terms of its caustics, though we may conjecture that this lower limit is comparable to that for other predictions of the GTD for elastic waves. Achenbach *et al.* (1979a) made experimental

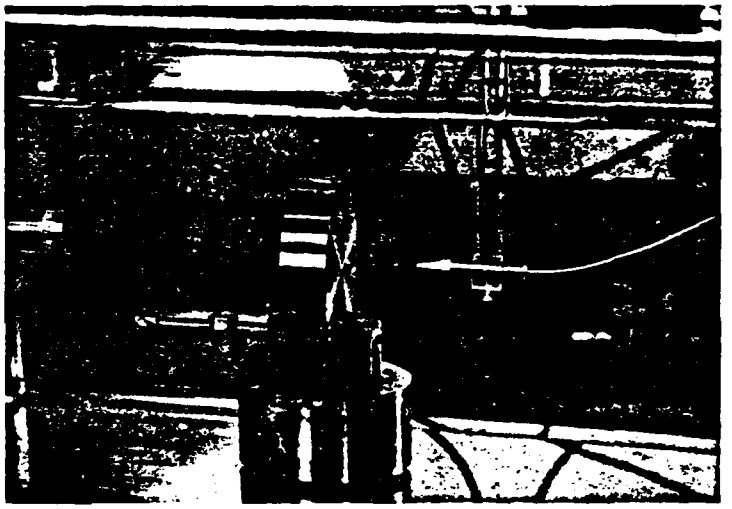

FIG. 17. Photograph of hydrophone, tank, transducer, and titanium disk.

comparisons, with this elastodynamic theory, of the angular and frequency spectra for diffraction by a circular disc. They found good agreement for l/λ down to 0·8, which was the lowest available in their experiments (corresponding to 2 MHz P-waves in Ti with crack radius $l = 2{\cdot}5$ mm). Thus while further confirmation is needed, the regime $l/\lambda > 1$ may be provisionally considered appropriate for caustics, so our comments in this subsection are mainly concerned with this regime.

One specialized approach to data inversion using physical elastodynamics, suggested by Achenbach *et al.* (1979a), is to compare experiment with the theoretically predicted periodicity of the peaks in the frequency spectrum for scattered P-waves, which are identified as the first arriving pulses. This approach requires the *a priori* knowledge that the incident wave lies in a plane of symmetry of a planar crack; given this knowledge, the radius of an artificial circular defect was accurately determined. On examination of earlier successful comparisons of experimental angular and frequency spectra with scalar wave GTD (Adler and Lewis, 1976), it appears that the spacing of interference P-waves peaks is only moderately influenced by elastic wave properties.

Another inversion technique using GTD (Achenbach *et al.*, 1979b) involves the application of Fourier-type inversion integrals to the amplitude of P-waves scattered by a planar crack. To date, this method has needed *a priori* knowledge of the crack plane, or at least of a plane of symmetry in which source and receiver can be located. Data from the experiments mentioned above using a 2·5 mm radius circular crack have been successfully interpreted

using such an inversion integral. However, several steps are necessary before a technique of this type—which requires quantitative measurement and interpretation of the scattered field—can measure the shape, size and orientation of a real crack. Firstly, still assuming a planar crack, the problem becomes three-dimensional if there is no prior knowledge of the orientation or symmetry; this generalization is amenable to an inversion integral approach, at the expense of complexity. Next, once the assumption of a planar crack is removed, a probabilistic analysis of the kind discussed by Richardson (this Volume, Chapter 5) becomes an essential part of the inversion. This analysis would require support by forward scattering calculations from non-coplanar cracks, to estimate the intrinsic error introduced by variations in crack roughness. Finally, the faces of real cracks, notably fatigue cracks, are often partially closed and therefore partly transparent to ultrasound, especially in the presence of residual compressive stresses. For an assembled structure, these stresses depend in turn on material type, crack growth history, the amount of stress relaxation and induced stresses (Yee *et al.*, 1974). Another way to express the difficulty caused by crack closure is that the stress on the closed parts of the faces is not generally zero, so the GTD diffraction coefficients, derived by Achenbach and Gautesen (1976) using diffraction by a stress-free half-plane crack, are inappropriate. Therefore, this problem of crack closure, as with that of roughness, does not appear amenable to a deterministic inversion integral approach. It is worth remembering, however, that it is precisely these properties of real cracks that render acoustical images difficult to interpret even for large cracks, thereby providing much of the motivation for seeking inversion procedures for high frequency scattering.

Let us now speculate on the influence of these difficulties on the caustics approach for real cracks. Firstly, if a crack is known to be planar, its plane can in principle be determined provided access is available to the near field. If the crack is non-coplanar, the far field caustic still yields the crack projection in the incident beam direction; the detailed topology of the crack faces does not influence the caustic geometry, so that crack surface roughness is not a problem. Concerning crack closure, first note that even for a high NDT ultrasonic intensity of $100\,\mathrm{kWm}^{-2}$, the actual displacement amplitude is only about 10 Å for 10 MHz *P*-waves in steel. Recent fracture studies by Bowles (1978) on Al alloys show that the crack tip is generally elliptical and open by several μm. Therefore for these cases the edge of the crack is opaque to ultrasound, so the caustic can be formed by the edge. For an unloaded crack, typically less than 20% of the faces are actually closed; therefore "false" edges inside the crack are much smaller, so their caustic will also be much smaller and either unresolved or else easily distinguished from the caustic from the "true" edge. The price to be paid by the caustics method for crack closure is in a reduction of the contrast (or signal/noise ratio) available experimentally,

rather than in the theoretical interpretation. From this discussion, it appears that much of the difficulty of extending inversion from artificial to real cracks is avoided by the caustics method. The one remaining question concerns irregularity of the edge itself, which can for example be pinned by local inhomogeneities; this is an important problem for future investigation. Since there is almost a one-to-one correspondence between points on the caustic section and points on the edge projection, it may be possible to derive information on some parts of the projection even though other parts are too irregular and hence unsuitable for well-defined caustics.

A different approach to inversion, applicable in the regime $l/\lambda > 1$ as well as elsewhere, is the adaptive learning method (Whalen and Mucciardi, 1979). Here, a computer is "trained" on either experimental data from known defects, or calculations based on theoretical scattering models. For cracks, the model used was the GTD. The size and orientation of artificial elliptical cracks were determined by using the calculated far field frequency spectrum at several scattering angles as input to the programmes, which select the best fit from these theoretical data (Whalen *et al.*, 1979). The method has also been used to derive defect size and orientation from scattering by artificial ellipsoidal voids. A list of the various theoretical models used, with appropriate further references, is given in a review by Kino (1979); most of these models are only valid in the regime $l/\lambda < 1$, which is outside the scope of this comparative discussion because there are then no caustics. One advantage of adaptive learning methods is the ability to distinguish volumetric from crack-like defects using far field measurements; we have seen in Section V.*A* that this distinction is only possible in general for our present method using the topology of the near field caustic, though a flat crack can be identified among other defects by rotation, as described in Section III.*A*. On the other hand, much difficult work remains for adaptive learning concerning inversion for real cracks, e.g. the influence of crack face roughness and closure, and it is not yet clear how well such problems can be overcome. In addition, these computing methods do not bring out the physical implications of features in the diffracted field as well as analytical approaches such as those of Achenbach *et al.* (1979b) discussed above, or the caustics method.

This subsection has concentrated on inversion for $l/\lambda > 1$ by analytical or numerical interpretation of the scattered amplitude, which includes ultrasonic spectroscopy (e.g. Adler *et al.*, 1977) as one form of data presentation. In a sense, the interpretation of any ultrasonic measurement which leads to quantitative parameters of the defect is at least a partial inversion procedure. An extensive literature exists in this area, which is not discussed here; reviews for cracks have been given by Doyle and Scala (1978) and Coffey (1979) (see also Tittman *et al.* (1980) for recent work). These specialized techniques are often important and attractively simple, particularly those based on pulse

transit-time measurement, but they are not designed to yield the complete shape and size of unknown defects, as is the case for caustics. We also omit discussion of the regime $l/\lambda < 1$, for which the diffracted field is dominated by interference effects rather than the geometrical coalescense of rays; appropriate references can be pursued beginning with the review by Kino (1979).

In conclusion, we summarize the principal attractive features of the caustics method for the inversion of ultrasonic scattering data, provided of course that the caustic section can be identified in a particular experiment:

(1) The procedure is simple, and easily understood in terms of diffraction effects. There is a close correspondence between features of the caustic and parts of the edge projection.
(2) A detailed measurement of amplitude and phase is not needed—only the location of local intensity maxima. Therefore signal deconvolution, e.g. for the frequency response and coupling of the receiver, is not necessary.
(3) No spectral analysis is required, though gating out low frequencies would improve the sharpness and hence ease of identification.
(4) Caustics occur for either continuous or pulsed ultrasound; pulses offer elimination of mode-converted waves by timing methods.
(5) The technique can handle tilted or non-coplanar cracks.
(6) The analytical complications of elastic wave theory compared with scalar (acoustical) wave theory are avoided with no loss of validity.
(7) The extension from artificial to real cracks may be easier than for methods relying on a detailed measurement of scattering amplitude, since crack face roughness and closure do not influence the caustic geometry.

Appendix: Caustic Geometry from Tilted or Non-coplanar Cracks

The field points y lying on the caustic surface formed by a general convex edge, which need not be planar, satisfy eqns (6) and (7). Now picture a planar crack whose edge is the projection of the general crack in the direction of an incident plane wave (Fig. 18). The application of eqns (6) and (7) readily shows that the caustic formed by this planar crack satisfies eqns (9) and (10). We wish to show that in the far field, eqns (6) and (7) reduce to eqns (9) and (10), i.e., that the far field caustic from tilted or non-coplanar cracks is equivalent to that produced by the projection of the crack in the incident beam direction.

In order to evaluate derivatives, it is convenient to write eqns (6) and (7) in their expanded but equivalent forms

$$(\mathbf{y}-\mathbf{x})\cdot\frac{\partial \mathbf{x}}{\partial s} = |\mathbf{y}-\mathbf{x}|\cos\beta \tag{A1}$$

$$|\mathbf{y}-\mathbf{x}|\frac{\partial \cos\beta}{\partial s} + \sin^2\beta - (\mathbf{y}-\mathbf{x})\cdot\frac{\partial^2 \mathbf{x}}{\partial s^2} = 0 \tag{A2}$$

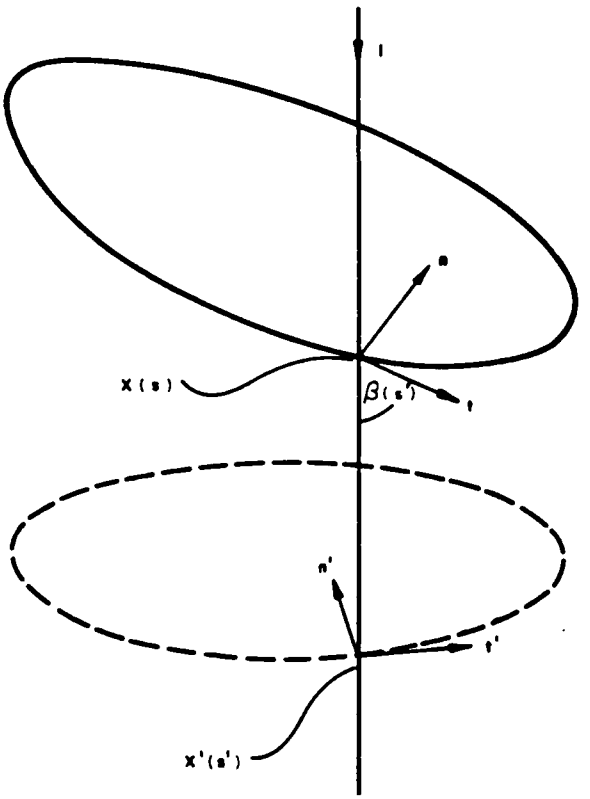

FIG. 18. Projection of a tilted or non-coplanar crack in the direction of an incident plane wave.

We now relate x and its derivatives to the parameters of the projection. From Fig. 5,

$$\mathbf{x} = \mathbf{x}\cdot\mathbf{i}\,\mathbf{i} + \mathbf{x}' \tag{A3}$$

Differentiation of eqn (A3), together with the relations $\partial \mathbf{x}/\partial s \cdot \mathbf{i} = \cos\beta$, $\partial \mathbf{x}'/\partial s' = \mathbf{t}'$, and $\partial s'/\partial s = \sin\beta$ yields

$$\frac{\partial \mathbf{x}}{\partial s}(=\mathbf{t}) = \cos\beta\,\mathbf{i} + \sin\beta\,\mathbf{t}' \tag{A4}$$

A second differentiation, using $\partial \mathbf{t}'/\partial s' = \mathbf{n}'/\rho'$ and eqn (A4) to eliminate $\mathbf{t}'$, gives

$$\frac{\partial^2 \mathbf{x}}{\partial s^2} = \frac{\partial \cos\beta}{\partial s}\mathbf{i} + \frac{\sin^2\beta}{\rho'}\mathbf{n}' + \frac{\partial \sin\beta}{\partial s}\left(\frac{\mathbf{t}-\cos\beta\,\mathbf{i}}{\sin\beta}\right) \tag{A5}$$

Substitution of eqns (A3) and (A4) into the ray eqn (A1) gives

$$(\mathbf{y}-\mathbf{x}')\cdot\mathbf{t}' = \cot\beta(|\mathbf{y}-\mathbf{x}| - (\mathbf{y}-\mathbf{x})\cdot\mathbf{i}) \tag{A6}$$

Substitution of eqn (A5) into the caustic eqn (A2) gives, using eqn (A1) and some algebra, the result

$$(\mathbf{y}-\mathbf{x}')\cdot\mathbf{n}' = \rho' \left[1-\frac{\dfrac{\partial\beta}{\partial s}}{\sin^3\beta}\{|\mathbf{y}-\mathbf{x}|-(\mathbf{y}-\mathbf{x})\cdot\mathbf{i}\} \right] \tag{A7}$$

Equations (A6) and (A7) reduce in the far field to eqns (9) and (10) as required, provided $|\mathbf{y}-\mathbf{x}|-(\mathbf{y}-\mathbf{x})\cdot\mathbf{i}\to 0$ in that region. We now show that this is a solution of eqns (A1) and (A2); it is equivalent to showing that $\hat{\boldsymbol{\sigma}}\cdot\mathbf{i}\to 1$ in the far field, i.e., rays to the caustic are asymptotic to the forward scattering direction.

We now write equations in terms of $\boldsymbol{\sigma}=\mathbf{y}-\mathbf{x}$ for brevity, since there is no further need to evaluate derivatives. Using eqn (A3) to eliminate $\mathbf{x}'$, the ray eqn (A6) can be written as

$$\hat{\boldsymbol{\sigma}}\cdot\mathbf{t}' = \cot\beta(1-\hat{\sigma}\cdot\mathbf{i}) \tag{A8}$$

Since $(\mathbf{i},\mathbf{t}',\mathbf{n}')$ form an orthonormal set, $\hat{\boldsymbol{\sigma}}\cdot\mathbf{i}\to 1$ is a solution of this equation—i.e., forward scattering rays exist (in the near field as well as the far field). Now using eqns (A4) and (A5), the caustic eqn (A2) can be written as

$$-\frac{\partial\cos\beta}{\partial s}(1-\hat{\boldsymbol{\sigma}}\cdot\mathbf{i})+\frac{\partial\sin\beta}{\partial s}\hat{\boldsymbol{\sigma}}\cdot\mathbf{t}'+\frac{\sin^2\beta}{\rho'}\hat{\boldsymbol{\sigma}}\cdot\mathbf{n}'-\frac{\sin^2\beta}{\sigma}=0 \tag{A9}$$

In the far field, $\hat{\boldsymbol{\sigma}}\cdot\mathbf{i}\to 1$ is a solution because then, $\hat{\boldsymbol{\sigma}}\cdot\mathbf{t}'$ and $\hat{\boldsymbol{\sigma}}\cdot\mathbf{n}'\to 0$ and, in that region, $\sin^2\beta/\sigma\to 0$. We conclude that the far field caustic from tilted or non-coplanar cracks is equivalent to that produced by the projection of the crack edge in the direction of an incident plane wave.

It is worth noting that there is a second far field solution to eqns (A1) and (A2), which is

$$\hat{\boldsymbol{\sigma}}\cdot\mathbf{i}\to 1-\frac{2\sin^6\beta}{\sin^4\beta-\sin^2\beta+(\rho'/\rho)^2}$$

We need not investigate in detail any implications of this solution, since it represents scattering widely dispersed in the far field. For normal incidence on a planar crack, it reduces to the backscattered caustic; for moderate departures from this case, it represents rays in the backscattered half-space.

V. Acknowledgement

The authors would like to thank Mike Buckley for initiating and continuing support for this project. We would like to thank M. A. Breazeale for his help and advice on this work. We would also like to express appreciation to D. W. Fitting for his contributions and to Maxine Martin for typing this manuscript.

The financial support of Defense Advanced Research Projects Agency, USA, and Aeronautical Research Laboratories, Australia, is also appreciated.

REFERENCES

Achenbach, J. D. and Gautesen, A. K. (1976). *J. Acoust. Soc. Am.* **61**, 413–421.
Achenbach, J. D., Adler, L., Lewis, D. K. and McMaken, H. (1979a). *J. Acoust. Soc. Am.* **66**, 1848–1856.
Achenbach, J. D., Viswanathan, K. and Norris, A. (1979b). *Wave Motion* **1**, 299–316.
Adler, L. and Lewis, D. K. (1976). *IEEE Trans. Sonics and Ultrasonics* **SU-23**, 351–356.
Adler, L., Cook, K. V., Whaley, H. L. and McClung, R. W. (1977). *Mat. Eval.* **35**, 44–50.
Berry, M. V. (1976). *Adv. Phys.* **25**, 1–26.
Bifulco, F. and Sachse, W. (1975). *Ultrasonics* **13**, 113–116.
Born, M. and Wolf, E. (1959). "Principles of Optics." Pergamon, London.
Bowles, C. Q. (1978). Delft University of Technology, Department of Aerospace Engineering Rep. LR-270.
Coffey, J. M. (1979). Central Electricity Generating Board Report no. NW/SSD/RM/65/79.
Conner, J. N. L. (1976). *Molec. Phys.* **31**, 33–35.
Coulson, J. and Becknell, C. G. (1922). *Phys. Rev.* **20**, 594–600, 607–612.
Courant, R. and John, F. (1965). "Introduction to Calculus and Analysis," Vol. I. Wiley, New York.
Doyle, P. A. (1980). *J. Phys. D: Appl. Phys.* **13**, 163–177.
Doyle, P. A. and Scala, C. M. (1978). *Ultrasonics* **16**, 164–170.
Keller, J. B. (1957). *J. Appl. Phys.* **28**, 426–444.
Kino, G. S. (1979). *Science* **206**, 173–180.
Kline, M. and Kay, I. W. (1965). "Electromagnetic Theory and Geometrical Optics," Chapter 8. Interscience, New York.
Korpel, A. (1968). *IEEE Trans. on Sonics and Ultrasonics*, **SU-15**, 153–157.
Kravstov, Yu. A. (1964). *Radiofiz.* **7**, 664–673.
Ludwig, D. (1966). *Comm. Pure and Appl. Math.* **19**, 215–250.
Martin, F. D., Adler, L. and Breazeale, M. A. (1972). *J. Appl. Phys.* **43**, 1480–1487.
Mathews, J. and Walker, R. L. (1964). "Mathematical Methods of Physics," pp. 380–382. Benjamin, New York.
Nye, J. F. (1978). *Proc. Roy. Soc.* **A361**, 21–41.
Pearcey, T. (1946). *Phil. Mag.* **37**, 311–317.
Poston, T. and Stewart, I. N. (1978). "Catastrophe Theory and Its Applications." Pitman, London.
Skudrzyk, E. (1971). "The Foundations of Acoustics". Springer-Verlag, Berlin.
Sommerfeld, A. J. W. (1954). "Optics." Academic Press, New York.
Thom, R. (1975). "Structural Stability and Morphogenesis." Benjamin, Reading, Mass.
Tittmann, B. R., Buck, O., Ahlberg, L., De Billy, M., Cohen-Tenoudji, F., Jungman, A. and Quentin, G. (1980). *J. Appl. Phys.* **51**, 142–150.
Trinkaus, H. (1971). *Z. Angew. Phys.* **31**, 229–235.
Whalen, M. F. and Mucciardi, A. N. (1979). Interdisciplinary Program for Quantitative Flaw Definition, Semi-Annual Report, 98–111.
Whalen, M. F., O'Brien, L. J. and Mucciardi, A. N. (1979). ARPA/AFML Review of Progress in Quantitative NDE, in press (as in AFML report).
Yee, B. G. W., Couchman, J. C., Hagemeyer, J. W. and Chang, F. H. (1974). *Non-destructive Testing* **7**, 245–250.

INVERSION OF SCATTERING DATA OF THE SHADOW REGION OF DISCONTINUITIES*

Laszlo Adler, Jerry Latimer† and Lynn Congos
Department of Welding Engineering
Ohio State University
190 W. 19th Avenue
Columbus, Ohio 43210

and

Peter Doyle
Aeronautical Research Laboratories
Melbourne, Australia

ABSTRACT

To obtain geometrical characteristics of defects a theory has been formulated [P. A. Doyle, J. Phys. D: Appl. Phy. 13: 163-77 (1980)] which considers the caustic pattern created by diffraction from the edge of a crack like defect. Model experiments were carried out to observe ultrasonic caustics in the shadow of obstacles using a 250μ diameter miniature broad band probe as a detecter. Other techniques are also considered. Qualitative agreement has been obtained between experiment and theory.

INTRODUCTION

The central problem for ultrasonic NDE is to develop methods for the inversion of scattering data. It was pointed out by Doyle (1979, 1980) that there is an attractively simple relationship between the geometry of the edge of a crack or other defect, and the geometry of the caustic enveloping the rays diffracted once by that edge. This inversion procedure offered a number of attractive features, perhaps most importantly the hope of avoiding problems due to crack face roughness and closure, which are serious difficulties for any technique relying on a detailed measurement of the amplitude and phase of diffracted rays. Another advantage is that only the geometry of caustics is required, allowing the interpretation of elastic wave scattering in terms of scalar wave theory.

Caustics of diffracted rays are well known in optics, as well as in some other fields of scattering characterized by large values of ka. For optics, the classic illustration is the formation of a bright asteroid in the region of geometrical shadow behind an elliptical obstacle (Coulson and Beckell 1922). Our present question is whether similar caustics can be observed by diffraction of ultrasonic waves, for which the typical values of ka are of course much smaller. The first step towards answering this question has been given by Doyle (1980): by considering the Airy fringes clothing the position of an ordinary point on the caustic (an 'elementary fold' catastrophe), it was found that the typical contrast (≈ several ∂B) and width (≈ 1-1.5 wavelengths) should be adequate for observation. It is the purpose of this paper to discover more precisely the region where the caustic of singly scattered rays occurs, and to present preliminary observations using artificial scatterers.

Location of the Caustic

We know from earlier work that when it occurs, the caustic of singly scattered rays is always in or at least centered in the geometrical shadow region. In addition, general limitations placed on the shape of the caustics by the application of catastrophe theory (Doyle 1980) require that for a purely convex crack, a section through the caustic must consist of a closed line interrupted only by cusps. Therefore we know what to look for, and to some extent at least, where to look. On the other hand, it is clear that the caustic will not remain visible for an indefinite distance behind the object. For example, for normal incidence of a plane wave on some planar object, the diffracted field in the 'shadow' must eventually return to equal the incident field, as described for scalar waves by the forward scattering amplitude in Fraunhofer diffraction. Equivalently, thinking of the scattering as a diffusion process, energy will spread back across the shadow boundary, eventually obliterating the shadow and any field structure within it.

To more precisely define the range from an object within which caustics are expected, consider a plane acoustical wave incident normally in the direction $\underset{\sim}{i}$ on a planar disc of typical dimension a, in the Kirchoff approximation (Fig. 1). Adapting the Rubinowitz representation of the Kirchoff integral for the complementary aperture problem (e.g. Born and Wolf 1959) by the use of Babinet's principle, the field diffracted by a disc to the point $\underset{\sim}{y}$ can be written as

$$u(\underset{\sim}{y}) = u^{(g)}(\underset{\sim}{y}) + u^{(d)}(\underset{\sim}{y}) \qquad (1)$$

where $u^{(g)}(\underset{\sim}{y}) = 0$ for $\underset{\sim}{y}$ in geometrical shadow and $= 1$ outside.

$$u^{(d)}(\underset{\sim}{y}) = + \frac{1}{4\pi} \int_{\text{edge}} \frac{\partial \eta \exp[i(k\sigma+\phi_0(s))]\, \partial s}{\sigma(1 - \partial \cdot \underset{\sim}{j})} \qquad (2)$$

Here, $\underset{\sim}{\sigma}$ is the vector from an edge point to the field point $\underset{\sim}{y}$, having direction $\hat{\sigma}$ and magnitude σ. The normal $\underset{\sim}{n}$ strictly refers to the shadow boundary formed by the disc, but for the case considered, it is equivalent to the inward normal to the edge. The phase of the wave incident at s is $\phi_0(s)$, which is constant for the present case. This representation separates the diffracted field from the geometrical optics field; there is a discontinuity in $u^{(d)}(\underset{\sim}{y})$ caused by the change of sign of the denominator, which exactly cancels the discontinuity of the geometrical field $u^{(g)}(\underset{\sim}{y})$.

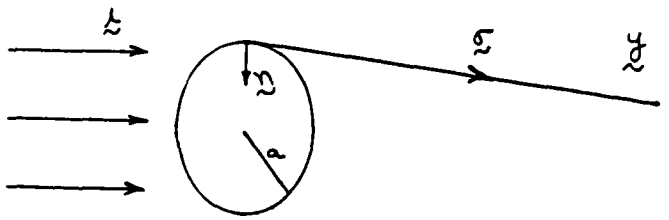

Fig. 1. Geometrical definition of parameters.

The diffraction integral (2) can be evaluated by stationary phase methods provided (A) the phase $(k\sigma + \phi_0)$ varies sufficiently rapidly with s for the stationary phase points to be well defined, and (B) the kernel of the integral remains substantially constant near the stationary points. For a larger scattering angle (say 30°), these conditions are both satisfied provided a/λ has at least some particular value. But in the geometrical shadow region, $k\sigma(s)$ clearly varies less as y is moved away from the disc, which implies that the stationary phase evaluation in or near the shadow is valid only within some finite distance. This limitation has been quantified by evaluating equation (2) uniformly across the shadow boundary using an auxiliary function (e.g. Skudrzyk 1971), which gave $u^{(d)}(y)$ in terms of a Fresnel integral. This integral can be expanded asymptotically to give as its first term the non-uniform evaluation of equation (2) by the stationary phase method. The result is that the ordinary stationary phase result is valid when

$$a/\lambda \gtrsim 2 \qquad (3)$$

and

$$\sigma \lesssim \frac{(\sigma.n)^2}{2\lambda} \qquad (4)$$

Equation (3) corresponds to the usual requirement that the object is not too small for the application of high frequency methods. Equation (4) means that the stationary phase method is only valid within the region shown in Fig. 2. Note that the parabolic "spreading" of the two shadow boundaries cross at $\sigma_N = a^2/2\lambda$, which happens to correspond to the last zero of intensity on the axis of the Fresnel diffraction pattern of a circular disc: this results because the transition from Fresnel to Fraunhofer diffraction for a plane incident wave involves similar considerations of the phase function in the Kirchoff integral.

At a distance beyond $\sigma = \sigma_N$, the field in the shadow region can no longer be considered as made up of rays from the stationary phase points, but rather as due to rays from all edge points. But these rays from stationary points are precisely in the direction of those predicted by Fermat's principle, as envisaged in the geometrical theory of diffraction (GTD). Therefore beyond $\sigma = \sigma_N$ in the shadow the GTD is also invalid. The absence of geometrical rays beyond σ_N also implies the absence of their coalescence, i.e., of caustics. Therefore caustics from singly scattered rays, which are expected in or near the shadow region, only occur within about σ_N of the object.

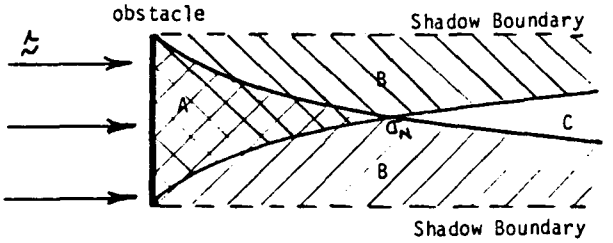

Fig. 2. Validity of stationary phase methods in shadow region.
A - Valid
B - Valid only for rays from opposite edge
C - Invalid

The optical experiments of Coulson and Becknell (1922) provide evidence for this interpretation. They photographed the shadow region of an elliptical disc for three different values of σ/σ_N. Firstly, for $\sigma/\sigma_N \simeq 1/13$, the caustic formed a sharply defined asteroid. But for $\sigma/\sigma_N \simeq 5$, a completely different pattern was observed. In this case, the simple Fraunhofer pattern did not occur, since these experiments used a point source of white light within the near field on the other side of the object. The third case considered corresponded to the intermediate value $\sigma/\sigma_N \simeq \frac{1}{4}$. There, the overall caustic asteroid was clearly visible, but the Airy fringes clothing it were more spread out. In addition, the cusps on the major axis had already merged with the edge: this is consistent with the view that for these cusps, the value of $(\underset{\sim}{\sigma}.\underset{\sim}{n})$ is a minimum, so this will be the first part of the caustic to disappear (cf. equation 4). On the other hand, the caustic near the minor axis is clearly visible right up to the shadow boundary, as would be anticipated because this part of the caustic originates from stationary points on the opposite side of the ellipse, which implies a larger $(\underset{\sim}{\sigma}.\underset{\sim}{n})$ value in equation (4).

By the discussion of this section, we have completed the definition of the region of the diffracted field where ultrasonic caustics are expected. We now describe our preliminary experimental observations of the shadow region of obstacles for ultrasound.

Experimental Observations. Preliminary experiments have been carried out to investigate the shadow region of circular and elliptical defects. The experiments may be divided into two complementary areas of investigation. First, circular and elliptical disks in water were used to demonstrate some of the essential features of the diffraction

field. Second, the shadow region of defects in diffusion bonded titanium were briefly considered in order to verify the potential usefulness of these techniques in nondestructive evaluation.

Diffraction by Circular and Elliptical Disks in Water. Both circular and elliptical disks were used as diffracting objects. The circular disk was constructed of two thin quartz disks which were cemented to a rubber O-ring. The diameter of the quartz disk was 2.54 cm. A small brass rod with a diameter of 1.6 mm was attached to one side of the structure in order to provide support. The essential feature of this composite structure was the air gap in the middle which blocked transmission of ultrasound into the shadow region.

The elliptical diffraction disk was constructed from two identical ellipses separated by a spacer. The ellipses and spacer were cut from an aluminum sheet having a thickness of .58 mm. The spacer placed between the two ellipses provided an air gap. The composite structure was held together with waterproof cement. The edges of the structure were machined to form a sharp edge around the periphery. A small stainless rod having a diameter of .3 mm was attached to one side of the structure for support. The length of the major axis was 2.54 cm and the length of the minor axis was 2.08 cm.

The shadow region was scanned with a miniature hydrophone. The active receiving element of the probe consisted of a piezoelectric disk with a diameter of 250 μm. Electronic buffering and amplification were built into the body of the hydrophone in order to maintain a good signal to noise ratio and a flat frequency response. The receiving element of the probe was mounted at the apex of a cone with an acoustically absorptive center. This design along with the small size of the sensing element minimized the interference by the probe with the acoustic field. A micromanipulator mounted on the observation tank permitted precision movements of the hydrophone to be made along three mutually perpendicular axes. The position of the hydrophone was read to within .1 mm by means of vernier scales. The output from the hydrophone was read from the peak to peak signal on an oscilloscope connected to the hydrophone preamplifier.

RESULTS

To demonstrate the presence of ultrasonic caustics an elliptical disk with axis 25.4 mm and 20.8 mm was used as "discontinuity". An approximately plane incident wave front was achieved by placing the obstacle in water in the far field of a focused transducer of nominal frequency 1 MHz (λ = 1.5 mm in water). The value of σ_N is 40 mm so a set of linear scans parallel to the minor axis was taken just 16 mm behind the object. A strong peak of intensity was observed on the major axis at the exact location predicted by theory for this cusp, which expected to be the strongest part of the caustic. On Fig. 3, the theoretical caustic and the experimental peak points are shown with reasonable agreement between theory and experiment. On the other hand, we do not yet have unambiguous identification of cusps on the upper half of the ellipse. This may be due to the supporting rod an additional source of scattering. Initial experiments were also carried out to study the shadow region of penny shaped cracks in titanium slags. The Airy pattern has also been observed here as shown on Fig. 4. This shows some feasibility of applying these techniques to defects in metals. But clearly more experiments at the higher frequencies are needed to show the usefulness of ultrasonic caustics for the inverse problem.

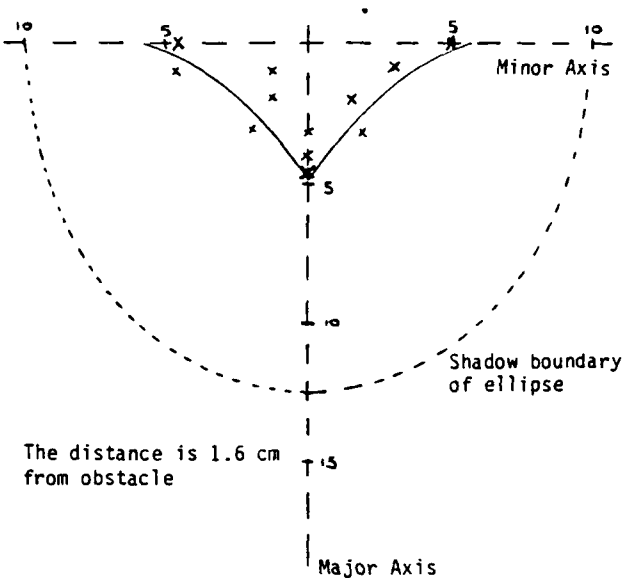

Fig. 3. Graph of predicted caustics versus peaks in observed scans parallel to the minor axis.

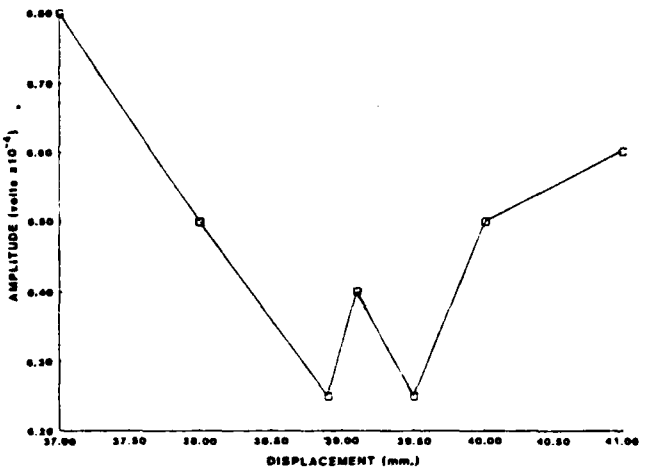

Fig. 4. Vertical scan through the shadow region of a 5 mm penny-shaped crack located in the center of a diffusion bonded titanium disk having a diameter of 10 cm and a thickness of 2-5 cm. The disk was oriented normally to the ultrasonic beam. The Arago spot is evident in the center of the diffraction pattern.

REFERENCES

Born, M. and Wolf, E. (1959). "Principles of Optics." Pergamon, London.

Coulson, J. and Becknell, C.G. (1922). Phys. Rev. 20, 594-600 and 607-612.

Doyle, P. A. (1979) DARPA/AF Review of Progress in Quantitative NDE, La Jolla, California.

Doyle, P. A. (1980) J. Phys. D. Appl. Phys. 13, 163-77.

Skudrzyk, E. (1971) "The Foundations of Acoustics" Springer-Verlag, Berlin.

Footnotes to the Title Page:

+ Present Address:
Department of Physics
University of Tennessee
Knoxville, Tennessee

* This work is supported jointly by the Defense Advanced Research Project Agency USA and by the Aeronautical Research Laboratories, Melbourne Australia.

DISCUSSION

W. Sachse (Cornell University) - Have you made any measurements on acoustics? I didn't see any results of the measurements of acoustics, but you showed it schematically.

L. Adler (Ohio State University) - What I showed you is the scanning behind the shadow region over the defect and the corresponding to maximum. I identified the two processes. The theory of diffraction to the crossing point, two crossing points, was indicated by the arrow. That was it.

W. Sachse - I had a student last year who tried something very similar to the experiment you outlined in the first part of your talk.

L. Adler - That was something similar to a Rayleigh tube using the large disc--

W. Sachse - No. Ours were about two centrimeters or so and these are actually one centimeter. There are various ones. For the circular elliptical disc the bright spots or acoustics were not very pronounced--you had to use a great deal of imagination.

L. Adler - Well, maybe we can discuss it. But if you recall, we had two maximum in the shadow region. That was for elliptical effect.

Observation of diffraction caustics for ultrasound

Rui-qi Dong and Laszlo Adler
Department of Welding Engineering, Ohio State University, Columbus, Ohio 43210
P. A. Doyle
Materials Division, Aeronautical Research Laboratories, Box 4331, P. O. Melbourne 3001, Australia

(Received 30 August 1982; accepted for publication 18 January 1983)

The formation of caustics due to the diffraction of ultrasound is observed by scanning in the shadow region close behind an elliptical obstacle in water. Good agreement is obtained between experiment and the theoretical geometry of the caustic, which is an astroid centered in that shadow region.

PACS numbers: 43.35.Cg

The formation of caustics due to the coalescence of diffracted light rays was demonstrated by Coulson and Becknell,[1] who photographed the field in the shadow region behind an elliptical or tilted circular disc. They found that the geometry of a section through the caustic surface was the evolute of the edge. This evolute/involute relationship is now well understood in terms of the geometrical theory of diffraction.[2] More recently, the topology of this caustic formed by edge diffraction has been classified[3] within the framework of the application of the catastrophe theorem to diffraction phenomena.[4,5] High resolution experiments[6] using a laser as a source have demonstrated the interference patterns called "diffraction catastrophes" associated with the classical caustic; in conjunction with the concept of wavefront dislocations,[7,8] these complicated patterns have been explained in minute detail.[6]

For acoustical or ultrasonic waves, the much lower frequencies compared with those in optics are less favorable to the formation of caustics, which are the dominant feature of wave fields in the high frequency limit. Nevertheless, approximate calculations[3] indicate that ultrasonic caustics should be observable by careful experiment; the present paper describes such observations for diffraction into the shadow region behind an elliptical disc in water.

The geometry of the experiment is shown in Fig. 1. A plane wave impinges normally in the z direction onto an elliptical disc of semiaxes a, b, and polar angle θ. The edge points $\mathbf{x}(s)$ of the disc are characterized by the arc length parameter s. The geometrical theory of diffraction states that a field point $P(\xi,\eta,z)$ receives a ray diffracted from $\mathbf{x}(s)$, and also lies on the caustic surface, provided respectively that the first and second derivatives, with respect to s, vanish for the ray path from $\mathbf{x}$ to P. It follows that the caustic surface has generators perpendicular to the disc, and a cross section called an astroid which is defined parametrically by

$$(\xi,\eta)=\left(\frac{(a^2-b^2)}{a}\cos^3\theta;\frac{-(a^2-b^2)}{b}\sin^3\theta\right). \quad (1)$$

The caustic does not persist for an indefinite distance behind the disc. For the incident plane wave simulated in the present experiment, the field in the "shadow" must eventually return to equal the incident field, as described for example by the forward scattering amplitude in Fraunhofer diffraction. Consequently, the caustic occurs only within approximately the near field $z<a^2/2\lambda$, where λ is the wavelength. Strictly, the original optical experiments[1] used a point source in the near field of the disc, rather than a plane wave. This caused no significant change in the geometry of the caustic from that defined by Eq. (1), though the quite different pattern observed in the far field has been explained only recently.[9]

Figure 2 illustrates the experimental arrangement. A focused transducer with a focal length of 70 mm was excited in a water tank at 5 MHz by a single frequency pulse from an Arenberg generator, though we emphasize that because the caustic is a geometrical rather than an interference effect, a broadband pulse could also have been used. The elliptical disc was placed well behind the focus, so that the incident field approximated a plane wave. This disc was constructed from two identical ellipses cemented together by a spacer, all cut from thin aluminum sheet with a thickness of 0.58 mm. The resulting air gap prevented through-transmission of the incident wave. The edge of this composite structure was machined to form a sharp edge around the periphery, whose dimensions were $(a,b)=(13,9.3)$ mm. The structure was sup-

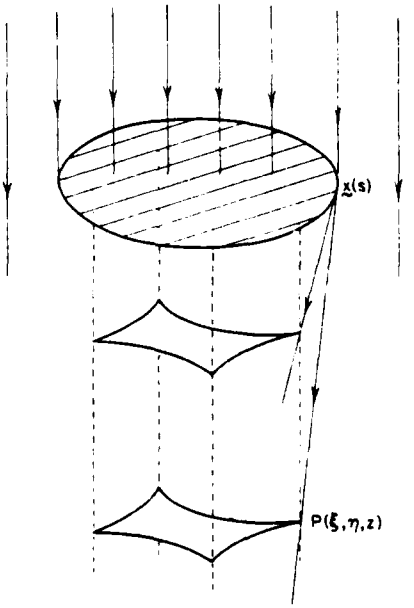

FIG. 1. The formation by edge diffraction of the caustic surface in the shadow region.

 0021-8979/83/052832-03$02.40

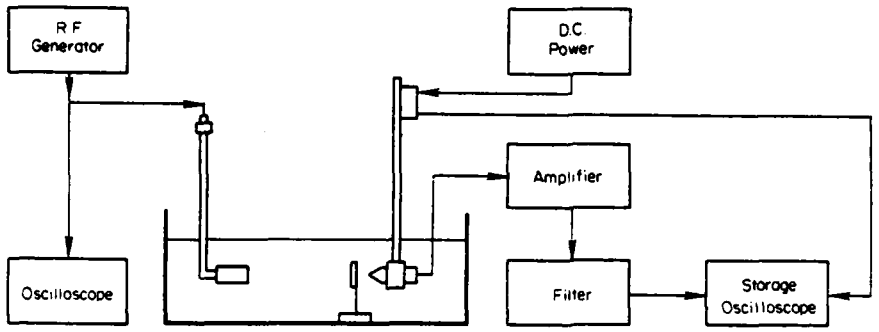

FIG. 2. Schematic of the experimental arrangement.

ported by a thin stainless steel rod of diameter 0.3 mm. The shadow region was scanned with a miniature hydrophone, in which the active receiving element was a piezoelectric disc of diameter 250 μm. Electronic buffering and amplification were built into the body of this hydrophone in order to maintain a good signal-to-noise ratio and a flat frequency response. The receiving element of the probe was mounted at the apex of a cone with an acoustically absorptive center. This design, along with the small size of the receiving element, minimized the interference by the probe with the acoustic field. A micromanipulator mounted on the observation tank permitted precision movements of the hydrophone along three mutually perpendicular axes, and position measurement to 0.1 mm by means of vernier scales. The output was displayed on a storage oscilloscope connected to the hydrophone preamplifier.

A sequence of scans across the shadow region along lines parallel to the minor axis are shown in Fig. 3. These scans were at a distance $z = 25$ mm behind the disc, which was well inside the near field for this case. No scans were taken in the lower half of the shadow, in order to avoid possible distortion due to diffraction by the support rod. The (ξ,η) coordinates of the hydrophone were determined directly using the vernier scales.

Small peaks can be seen inside the shadow region between the saturated bright field signals. The positions of these small peaks are plotted in the (ξ,η) plane in Fig. 4, and show good agreement with the position of the classical caustic (i.e., the astroid), both near the cusps and for ordinary points along the caustic. Therefore, we interpret these peaks as the first direct observation of the formation of diffraction caustics for ultrasound.

There seems little possibility, at the typical ultrasonic frequencies of several MHz, of observing the fine structure of the diffraction catastrophes associated with the caustic, because, unlike the optical case, it can be shown[3] that the typical fringe spacing involved is of the order of λ. Presumably, stronger caustics should occur at the higher frequencies used in ultrasonic microscopy, though approximate calculations[3] suggest that the expected contrast increases only as $\lambda^{-1/3}$.

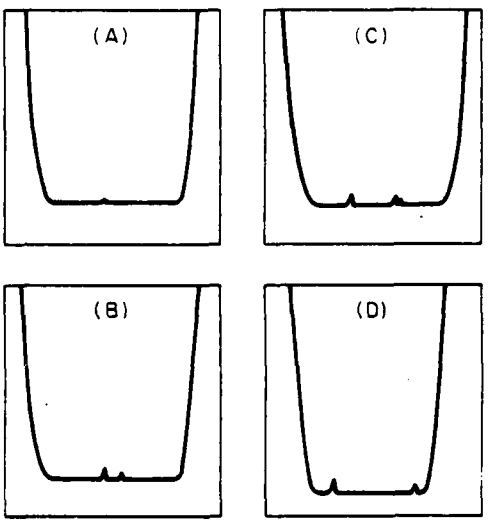

FIG. 3. Scans through the shadow region parallel to the η axis, i.e., the minor axis of the shadow. The η coordinates were as indicated on Fig. 4 and designated by A, B, C, D. The caustics are the small intensity peaks.

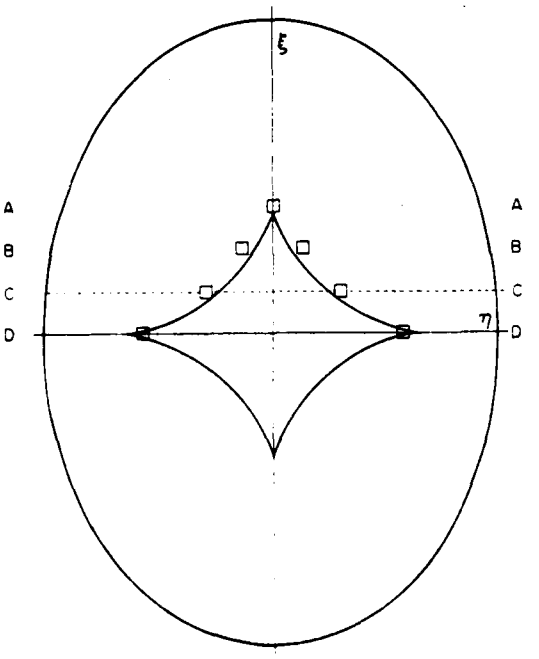

FIG. 4. Comparison of the positions of experimental peaks (marked □) and the theoretical astroid (solid line). The faint lines mark the coordinates of the scans in Fig. 3.

This work was supported by DARPA and ARL, Australia.

[1]J. Coulson and G. G. Becknell, Phys. Rev. **20**, 594 (1922); **20**, 607 (1922).
[2]J. B. Keller, J. Appl. Phys. **28**, 426 (1957).
[3]P. A. Doyle, J. Phys. D. **13**, 163 (1980).
[4]M. V. Berry, Adv. Phys. **25**, 1 (1976).
[5]T. Poston and I. N. Stewart, *Catastrophe Theory and its Applications* (Pitman, London, 1978).
[6]M. V. Berry, J. F. Nye, and F. J. Wright, Philos. Trans. R. Soc. London **291**, 453 (1979).
[7]J. F. Nye and M. V. Berry, Proc. R. Soc. London Ser. A. **336**, 165 (1974).
[8]J. F. Nye, Proc. R. Soc. London Ser. A. **378**, 219 (1981).
[9]P. A. Doyle (unpublished, 1982).

END

FILMED

4-84

DTIC